國立臺灣大學電機資訊學院電機工程學系

碩士論文

Department of Electrical Engineering
College of Electrical Engineering and Computer Science
National Taiwan University

Master Thesis

使用圓柱形標誌之體內光學追蹤應用於微創手術

Intracorporeal Optical Tracking of Instruments Using Cylindrical Marker for Minimally Invasive Surgery

曾彥翔

Yen-Hsiang Tseng

指導教授：陳永耀 博士

Advisor: Yung-Yaw Chen, Ph.D.

中華民國 103 年 7 月

July 2014

誌謝

轉眼之間，兩年的碩士研究生涯即將結束，而論文也已完成。這份論文能夠完成要感謝很多人，首先要感謝的是指導教授陳永耀教授，在研究方面，灌輸我作研究的邏輯架構，時常給予想法上的幫助，並且訓練自己想法不被框架限制住，補足了我在大學以前沒有歷練到的部分。感謝口試委員電機所連豐力教授，機械所顏家鈺教授，醫工所林文澧教授，以及醫學院何明志教授，在研究的方向上以及論文的寫作都給予我十分寶貴的建議。

感謝學長凱翔，除了研究的方法外，在實驗的設計以及器材的加工製作給予我很多幫助，節省了不少時間，品質也提升許多，在研究生涯中有你的幫助是相當幸運的。感謝昆翰，與你的討論常常可以得到突破性的想法，解決既有的瓶頸。感謝遵義，兩年中一起相處的回憶是十分具有紀念價值的。感謝宏恩、瑋如、卉萱，讓實驗室變的更歡樂，看到正在成長中的你們，就好像看到去年的自己。感謝助理郁文，幫我們處理上許多事務，使我們能夠在專注於研究上，不用為了事務的處理而煩惱。

感謝我的家人，在經濟方面，讓我不用為了生活而擔憂，可以專注於充實自己，在精神方面，給了我許多的支持，儘管因為研究減少了相處的時間，也沒有聽過你們埋怨，永遠是給予我支持與鼓勵，讓我沒有後顧之憂。最後，感謝所以幫助過我的人，沒有你們的幫助，研究的路上一定會過的更加艱辛，因此，這份論文完成的喜悅及榮耀將與你們一起分享。

中文摘要

目標：本論文致力於建立一套使用圓柱形標誌的體內光學追蹤系統，用於微創手術。目標是對於待追蹤物進行空間中的定位、追蹤，得知其空間位置後，可用於其他應用，像是擴增實境與危險警告。

方法：基於在 2013 年提出的體內光學追蹤系統下 [7]，改變標誌的形狀，由方形改為圓柱形。因原本的系統需將一個長方形的模具固定於待追蹤物上，再將方形標誌黏貼於模具上，然而，在手術中，此長方形模具接觸到組織時，模具上的銳角可能會對組織造成不必要的傷害。而本論文提出的圓柱形標記是黏貼於圓柱形的模具上，因此不會有銳角對組織造成傷害的疑慮。由於使用圓柱形標誌進行定位是一個新穎的想法，本論文也提出一個特定的演算法對圓柱形標誌進行標誌偵測。

結果：實驗證明，在 75 到 150 毫米的觀察距離內，此系統的平均定位誤差為 2.7 毫米，小於在微創手術中最大的安全距離上限：20 毫米。

結論：在本論文中提出的使用圓柱形標誌之光學追蹤系統可以完成在微創手術中的定位任務。此系統有三項優點：減少對組織不必要的傷害、可以進入更小的套孔，並且保留了體內光學定位系統的優點，包括較短的量測距離及更簡單的座標系統以減少座標轉換的誤差。

關鍵字：體內光學追蹤、圓柱形標誌、器械追蹤

ABSTRACT

Objectives: The aim of this thesis is to create an intracorporeal optical tracking system using cylindrical marker for minimally invasive surgery. The main function is to localize and to track the tracked objects, providing positions of the tracked objects, which can be used in other applications, like augmented reality and risk warning.

Methods: Based on the intracorporeal optical tracking system proposed in 2013 [7], shape of marker is improved from square to cylinder. In original system, it's necessary to attach a rectangular module rigidly to the tracked object. And the square marker can be affixed to the rectangular module. However, sharp edges of the rectangular module may give rise to unnecessary damages to tissues when it touches tissues in surgery. The cylindrical marker is affixed to a cylindrical module with no sharp edges. Hence, it can reduce unnecessary damages to tissues. Because using cylindrical marker to achieve tracking work is a novel idea, a specific algorithm to detect cylindrical marker is proposed in this thesis.

Results: The experiments shows that the mean error of tracking accuracy of the proposed system is 2.7 mm in observation distance from 75 to 150 mm, which is less than the maximal safe distance: 20 mm in minimally invasive surgery.

Conclusions: The novel optical tracking system proposed in this thesis using cylindrical marker can achieve tracking work for minimally invasive surgery. The system has three advantages: reducing unnecessary damages to tissues, feasibility to penetrate smaller trocar, and preserving advantages of intracorporeal optical tracking system, including shorter observation distance and simpler coordinate system to reduce errors caused by coordinate transformation.

Keywords: Intracorporeal optical tracking, Cylindrical marker, Instrument tracking

CONTENTS

LIST OF FIGURES

LIST OF TABLES

Chapter 1 Introduction

The aim of this thesis is to create an intracorporeal optical tracking system using cylindrical marker. The proposed system is based on intracorporeal optical tracking system using square marker, improving shape of the tracked fiducial marker from square to cylinder. In order to track using cylindrical marker, a specific marker detection algorithm is proposed.

Compared with optical tracking system using square marker, the marker modules used in the proposed system are cylinders, which can avoid unnecessary damages to tissues in surgery. On the other hand, due to larger useful area, the cylindrical marker modules can be used to achieve tracking work with a smaller size than which of square markers. That means instruments with cylindrical markers can penetrate smaller trocars compared with instruments with square markers. Besides, tracking system in this work preserves the advantages intracorporeal optical tracking system has.

The motivation and problem definition of this work is introduced in the following sections. A brief introduction of previous work and the proposed approach are introduced in this chapter.

1.1 Motivation and Problem Definition

Because the disadvantages of narrow view, complex hand-eye coordination, unintuitive operation, a restricted mobility and lack of information beyond the surface of organs, it contains difficulties for surgeons to perform a minimally invasive surgery. Hence, a computer-assisted system is needed. Intracorporeal tracking is a prerequisite to realize further assistance functions, like augmented reality or risk warning.

There are several technologies to realize tracking work, including kinetics robotics, extracorporeal optical tracking, electromagnetic tracking and intracorporeal optical tracking. Kinetics robotics provides acceptable accuracy, but it leads to operation interference. Extracorporeal optical tracking provides good accuracy. However, it’s not only expensive but limited by visibility. Electromagnetic tracking provides a simple structure and high accuracy, but the critical limitation is that it would be interfered by ferromagnetic material and electromagnetic signals. Among this technologies, intracorporeal optical tracking has advantages of no ferromagnetic interference, reducing observation distance and lower cost. However, markers used in previous intracorporeal optical tracking are plain square markers, which should be affixed to rectangular marker modules attached to instruments. The rectangular marker module may give rise to unnecessary damages to tissues when it touches tissues in surgery. To solve this disadvantage, the aim of this thesis is to build an intracorporeal optical tracking system

using cylindrical marker.

To achieve tracking work in minimally invasive surgeries, the tracking system this thesis proposed should meet high accuracy and real-time computation. And a specific design of cylindrical markers in needed because there is no previous work of tracking system using cylindrical marker in minimally invasive surgeries.

In summary, the aim of this thesis is to propose an intracorporeal optical tracking system using cylindrical markers to avoid accidental damages, and meeting high accuracy and real-time computation.

1.2 Previous Work

In 2008, Feuerstein et al. proposed an intraoperative laparoscope augmentation for port placement and resection planning [3]. The tracking technology used in their system can be classified into extracorporeal optical tracking system. A mount of multiple photoreflective spheres is attached rigidly to the instrument or the endoscope, shown in right of Fig. 1-1. Multiple infrared cameras are set on the ceiling of an operation room in order to get better sight view and to avoid occlusions, shown in left of Fig. 1-1. The position and orientation of the tracked target can be calculated when the infrared camera observing the photoreflective spheres.

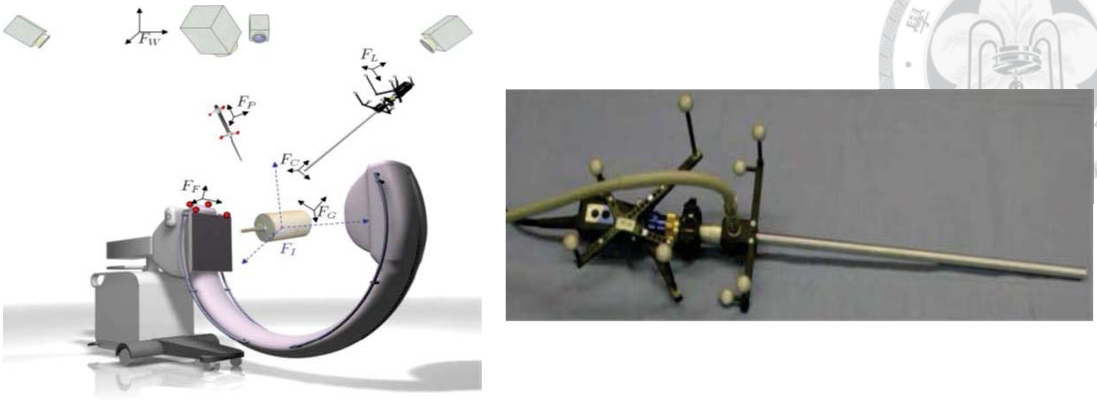

Fig. 1-1 System architecture of extracorporeal optical tracking system (left). The instrument within specific markers for optical tracking (right) [3].

In 2012, Langø et al. proposed a navigated laparoscopic ultrasound in abdomen [8]. The tracking technology used in the system is electromagnetic tracking. When the sensor fixed to tracked targets accepts magnetic signals form magnetic field generated by magnetic field generator, the system can calculate position of the sensor in generator coordinate system. It provides a simple and convenient structure and high accuracy. Nevertheless, the main issue is that the accuracy is interfered by ferromagnetic interference.

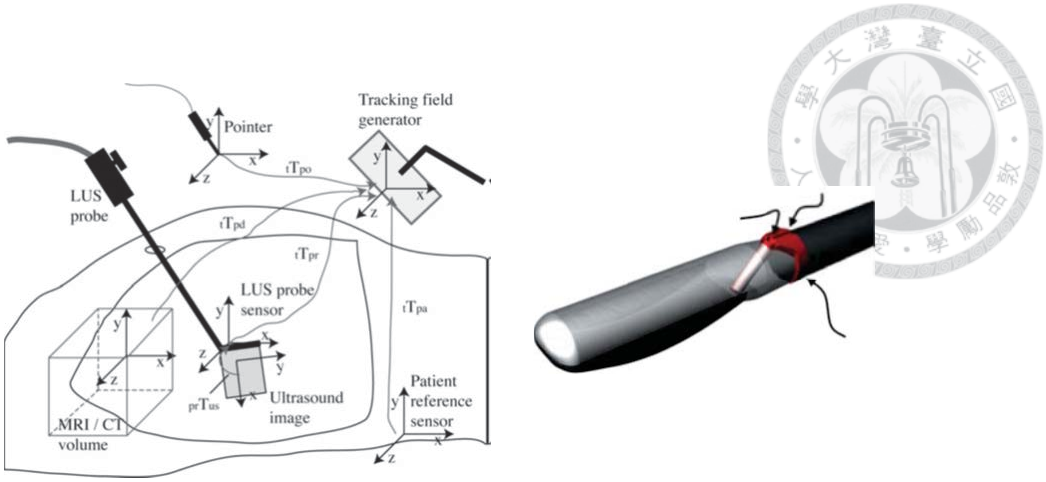

Fig. 1-2 System structure of electromagnetic tracking system (left) [8]. The EM sensor is settled rigidly to the tracked target (right).

In 2013, Ke et al. proposed an intracorporeal optical tracking system [7], shown in Fig. 1-3. The endoscope is adopted as image capture device. Square markers are affixed to rectangular marker modules attached to instruments. When the markers appears in images captured from endoscope, the system can calculate the transformation matrix from marker coordinates to endoscope coordinates using the specific marker patterns. Hence the tip position of instrument can be estimated by the transformation matrix and the relation between instrument tip and the markers. It's immune from ferromagnetic interference and achieve high tracking accuracy. However, the rectangular marker modules may lead to unnecessary damages to tissues when touching tissues.

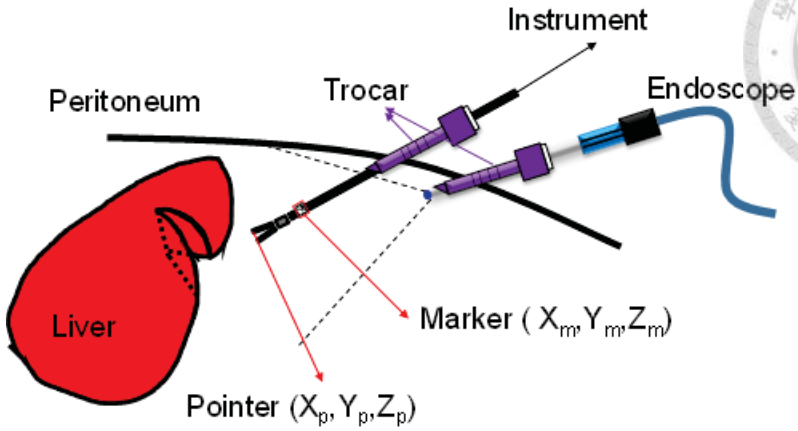

Fig. 1-3 The architecture of intracorporeal optical tracking system [7].

1.3 Proposed Approach

In this thesis, an intracorporeal optical tracking system using cylindrical marker is proposed. Based on the architecture of intracorporeal optical tracking system proposed in 2013, the shape of marker is improved from square to cylinder. The main advantage is to avoid unnecessary damages to tissues, which occurs when the sharp edges of rectangular marker module to which square markers is affixed touches tissues. There are less damages occurs when the cylindrical marker module touches tissues because there are no sharp edges existing on surface of cylindrical marker modules. On the other hand, it's a novel idea since there is no previous work using cylindrical markers to perform a tracking work.

Fig. 1-4　A cylindrical marker set is affixed to a cylindrical marker module which is attached to instrument.

As intracorporeal optical tracking system using square marker [7], the endoscope is adopted as image capture device. Because the endoscope has used in conventional minimally invasive surgery, there is no need for other specific sensor for this system. The cylindrical marker used in this system is a cylindrical marker set with many independent markers. Fig. 1-4 shows the marker set affixed to a cylindrical marker module which is attached to the instrument. It's a special design for marker detection. When endoscope captures image, the system detects possible marker sets, differentiates these possible marker sets and extracts features from these marker sets. The features and intrinsic parameters which are derived from off-line camera calibration are used to calculate transformation matrix from marker coordinates to camera coordinates, which is called extrinsic parameter matrix. Any position and pose of points in marker coordinate system can be transformed to position and pose in camera coordinate system using the extrinsic

parameter matrix. By these procedures, instruments or other tracked targets to which cylindrical markers are affixed can be tracked as long as the markers are detected by the tracking system. The overall flowchart is shown in Fig. 1-5.

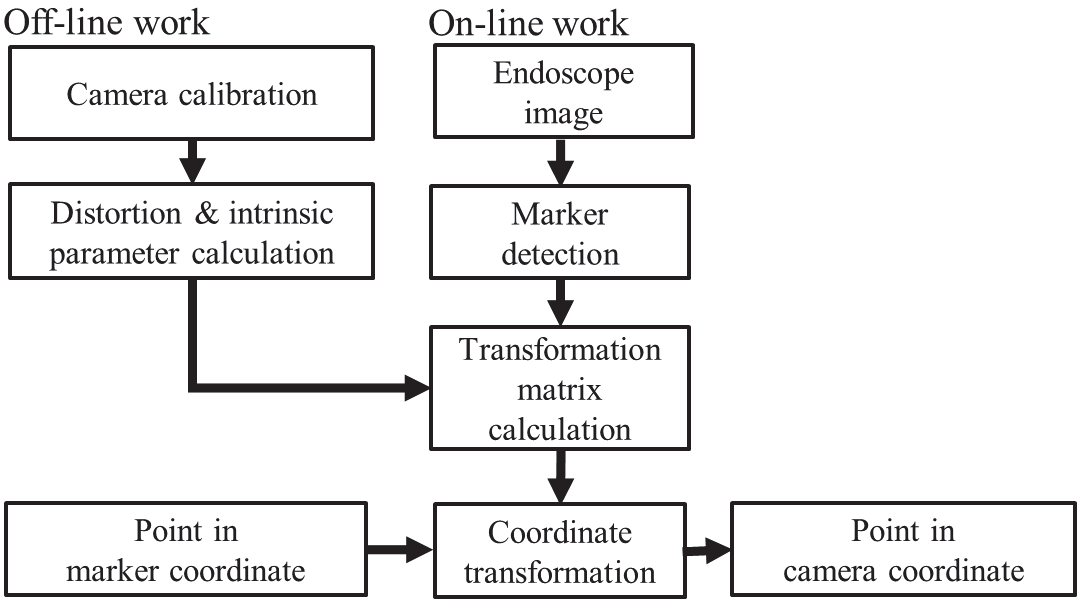

Fig. 1-5 Overall flowchart of intracorporeal optical tracking system using cylindrical marker.

The algorithm of transformation matrix calculation used in this system is the same with which in ARToolkit [1]. The ARToolkit system is designed for square markers. In order to adopt the algorithm of transformation matrix calculation from ARToolkit, the cylindrical markers are designed with some features to provide features which square markers can provide, including positions of 4 corner points, marker direction and marker id. The designed cylindrical marker is shown in Fig. 1-4.

The marker detection algorithm for square marker can't work for detecting cylindrical markers. Hence, a marker detection algorithm for cylindrical marker is proposed. Overall flowchart of marker detection algorithm for cylindrical marker is shown in Fig. 1-6. After marker detection, features of markers, including four positions of corner points, marker id and marker direction, are extracted. And these features can be used to calculate extrinsic parameter matrix.

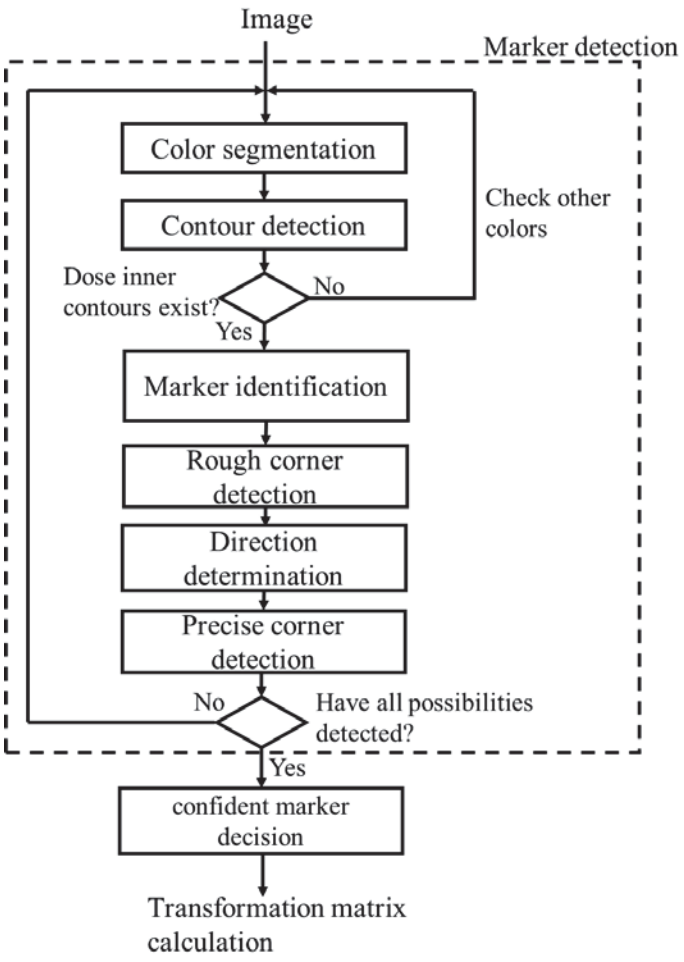

Fig. 1-6 Overall flowchart of marker detection algorithm for cylindrical marker.

Compared with intracorporeal optical tracking using square marker. The marker

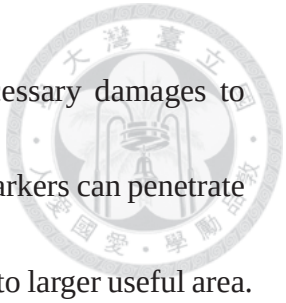

modules used in our system are cylinders, which can avoid unnecessary damages to tissues in surgery. On the other hand, instruments within cylindrical markers can penetrate smaller trocars compared with instruments within square markers due to larger useful area. Besides, tracking system in this work preserves the advantages intracorporeal optical tracking system has.

1.4 Thesis Overview

The structure of this thesis is as follows. The previous work of "***Tracking Technologies"*** used in minimally invasive surgery are reviewed and summarized in Chapter 2. Because the system this thesis proposed is based on intracorporeal optical tracking system using square marker, the architecture and tracking algorithm of ***"Intracorporeal Optical Tracking System Using Square Marker"*** are introduced in Chapter 3, and the differences between the two tracking system are also compared.

Chapter 4 introduces the design of ***"Intracorporeal Optical Tracking System Using Cylindrical Marker"***. System architecture, design of marker and marker detection algorithm are introduced. ***"Experimental Results"*** and analysis are shown in Chapter 5. A calibration between camera coordinate system and world coordinate system is built. The absolute accuracy of tracked positions relative to ground truth is verified. Finally, Chapter 6 gives ***"Conclusions and Future Work"*** of this research.

Chapter 2 Previous Work

Minimally invasive surgery is a highly complex medical task for surgeons because they have to deal with a complex hand-eye coordination, a narrow field of view and a restricted mobility. To solve these problems, image guidance technology was developed. The prerequisite for image guidance is to localize instruments and target structures like vessels and tumors. After that, the distance from instruments to risk or target structures can be measured and the information can be projected onto images using augmented reality technology. For this purpose, methods of tracking instruments are important elements for minimally invasive surgeries.

Tracking technology used in minimally invasive surgeries can be classified in to two categories according to the placement of sensor: extracorporeal and intracorporeal. Extracorporeal tracking can be classified into robot kinematics and optical tracking, which will be introduced in section 2.1. Intracorporeal tracking also can be categorized into three: electromagnetic tracking, optical tracking using stereo endoscope and optical tracking using traditional 2D endoscope, which will be introduced in section 2.2. Section 2.3 is the comparison of these tracking technologies.

2.1 Extracorporeal Tracking Technologies

The general extracorporeal tracking technologies can be classified into robot kinematics and optical tracking. Both of which are also used in other fields. The reason to classify this two technologies into extracorporeal tracking technologies is that the used sensors are set outside human body. Robot kinematics uses values derived from encoders and the pre-knowledge of the system to calculate positions of tracked targets, and the robot arm is set outside human body. The sensors used in optical tracking system are infrared cameras, which are attached to the ceiling of an operation room.

Robot kinematics technology is introduced in section 2.2.1. Extracorporeal optical tracking technology is introduced in section 2.2.2.

2.1.1 Robot Kinematics

Robot kinematics is a general tracking technology in minimally invasive surgeries from then until now [4, 9-12]. What should be tracked such as endoscopes or instruments are set to mechanisms. The mechanisms including encoders and mechanical arms can be divided into multiple coordinates according to joints linked by links. A configuration plot is shown in Fig. 2-1. Due to the known geometry information between each joint and link, the transformation matrix from each joint to near joint T_{i-1}^{i} can be calculated. A pose of target q^{i} in one coordinate system can be derived by multiplying the transformation

matrix T_{i-1}^{i} from the last coordinate system to this one by the pose of target in the last coordinate system q^{i-1}, shown in (2.1).

$$q^{i} = T_{i-1}^{i} q^{i-1} \tag{2.1}$$

A transformation matrix can be derived by other transformation matrices, shown in (2.2).

$$T_{1}^{n} = \prod_{i=1}^{n-1} T_{i}^{i+1} \tag{2.2}$$

Furthermore, transferred from first coordinate to the target coordinate, the pose of target in base coordinate system is obtained.

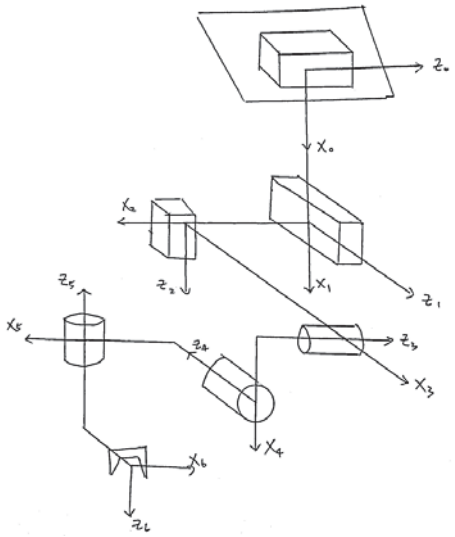

Fig. 2-1 Classic kinematics configuration, representing the relationship between each coordinate.

Fig. 2-2　Da Vinci surgical robot, with multiple robot arms [4].

This tracking technology is used in many systems. The most common case is Da Vinci robot system[4], shown in Fig. 2-2. Due to the need of high dimensional operations, the surgical robot has multiple robot arms and each arm has multiple joints, which makes it expensive. On the other hand, the position provided by the robot encoders is not accurate enough. One main reason is that the position of target is obtained from a lot of transformation, and each transformation generates some errors inevitably, which leads to large total errors. Another reason is when forces are applied to a surface or the trocars, the values derived from encoders are distorted significantly. Hence, robot kinematics technology is limited to become widespread for tracking in minimally invasive surgery. Even the Da Vinci system takes another tracking technology, visual tracking with stereo endoscopes, which will be introduced in 2.2.2.

2.1.2 Optical Tracking

Optical tracking system is a general tracking method in many fields. It's also applied to perform the tracking work for no only opening surgery but also minimally invasive surgery [2, 3, 13-20]. The illustration is shown in Fig. 2-3. To enhance the accuracy, the chose sensors are infrared cameras. The infrared cameras are set on the ceiling of an operation room in order to get better sight view. A mount of multiple photoreflective spheres is attached rigidly to the instrument or the endoscope like Fig. 2-4. When the infrared camera observing multiple photoreflective spheres of a tracked target, the system can calculate its position and orientation by triangular calculation.

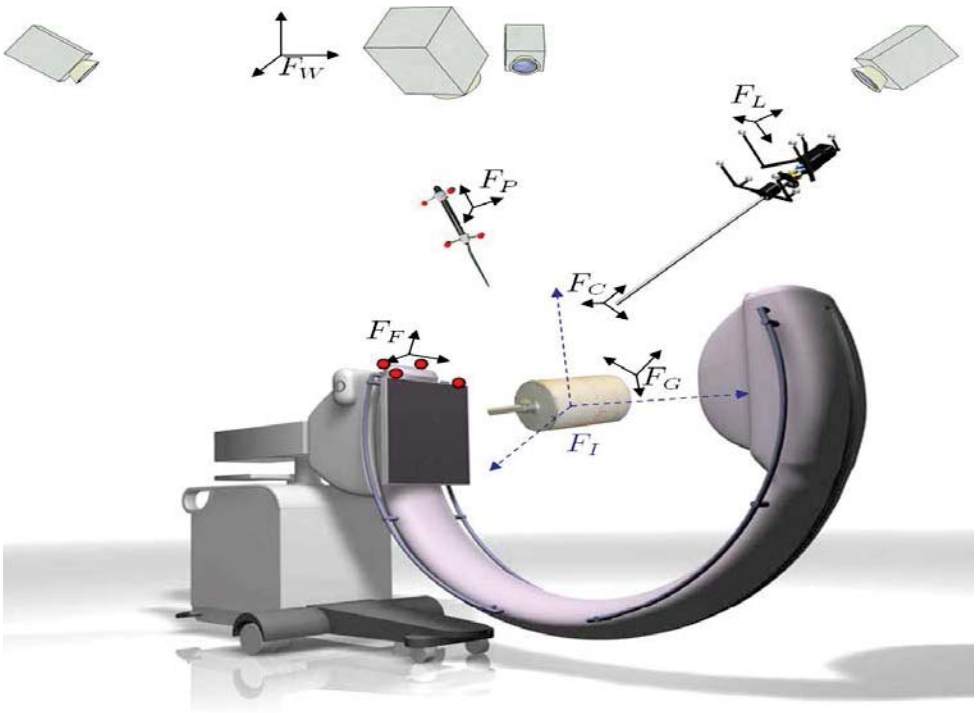

Fig. 2-3 Illustration of optical tracking system, including multiple infrared cameras and photoreflective spheres attached to the tracked target [3].

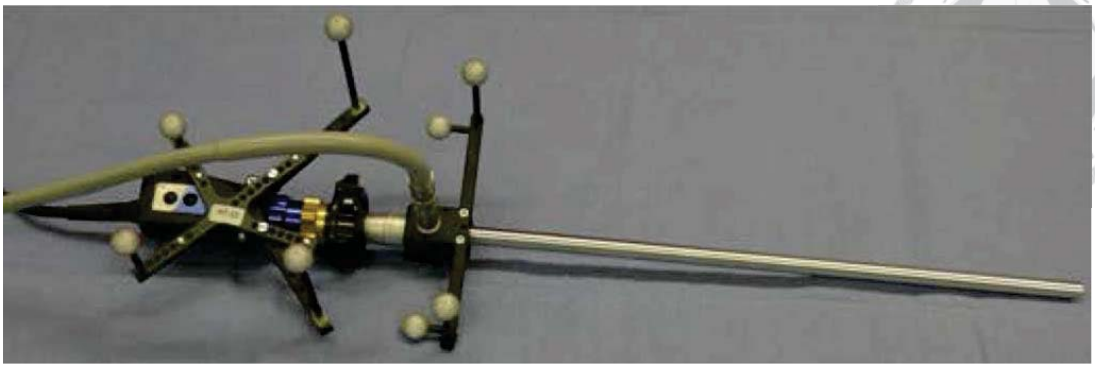

Fig. 2-4 Multiple photoreflective spheres are attached rigidly to the instrument [2].

Although this optical tracking system has satisfactory accuracy, there are some key points must be considered. First, once the sphere marker is occluded, the system can't track the marker. Also, it is usually occluded by medical personnel in an operation room. Thus, the system needs multiple cameras to make sure that the markers can be observed by at least one camera, which leads to larger cost of the system and difficulty to calibrate the camera coordinate systems. Second, also in order to enhance the accuracy, a large marker size is preferred. Nevertheless, the large size marker generates operation interference for surgeons to use the instruments.

2.2 Intracorporeal Tracking Technologies

Tracking technologies classified in intracorporeal tracking are three: electromagnetic tracking, optical tracking using stereo endoscope and optical tracking using 2D endoscope. The reason of the classification is sensors using in these three tracking technologies are placed inside human body, which would not lead to operation

interference for medical personnel.

Electromagnetic tracking technology is introduced in 2.2.1. Optical tracking using stereo endoscope is introduced in 2.2.2. And optical tracking using 2D endoscope is introduced in 2.2.3.

2.2.1 Electromagnetic Tracking

Electromagnetic tracking technology is one of the most promising means of localizing and tracking endoscopes or instruments. Many image guided surgery assistance system used it to track instruments and then performed navigation for augmented reality in minimally invasive surgeries [6, 8, 21-23]. However, interference from ferromagnetic material is the main issue for electromagnetic tracking system. Hence, some groups were dedicated to reduce electromagnetic tracking errors [24, 25].

A system structure of electromagnetic tracking system is shown in Fig. 2-5. It contains two main parts, magnetic field generator and magnetic field sensor. The magnetic field generator emits a magnetic field of a known strength, based on an alternating current. It is placed in a known location outside human body. It must be ensured the magnetic field generated can cover all work space of the tracked target. The sensors are fixed rigidly to the tracked target like Fig. 2-6. When the sensors are placed inside the magnetic field, unique voltages are induced. And the system can calculates the position and orientation of the sensors using the induced unique voltages.

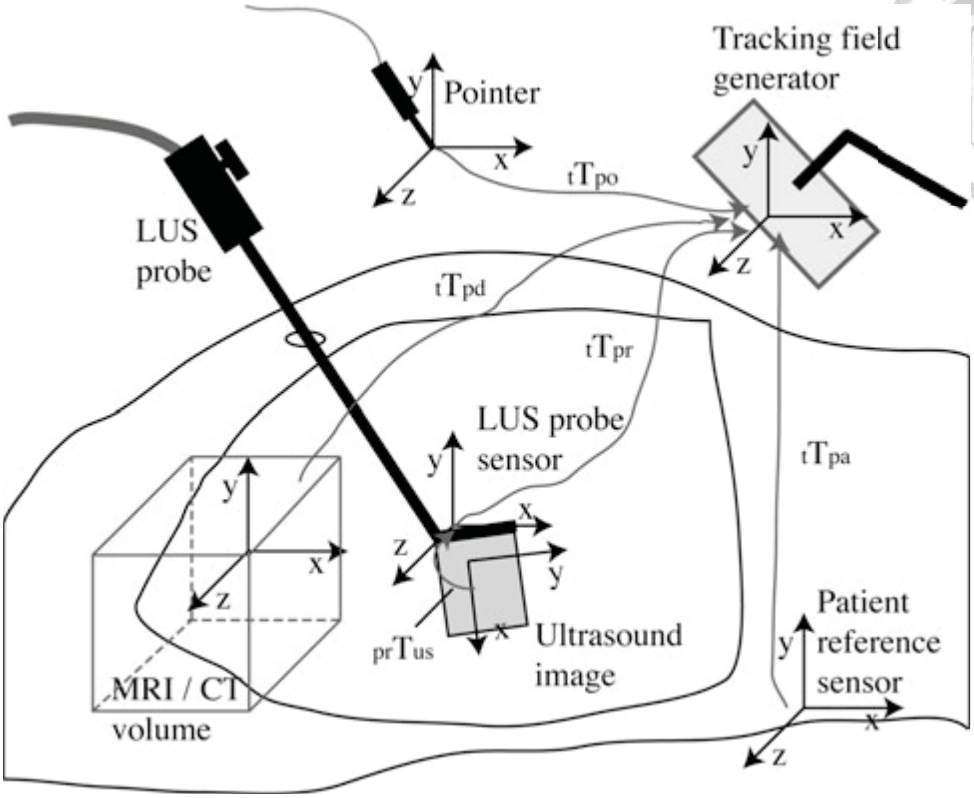

Fig. 2-5 System structure of electromagnetic tracking system [8]. The EM sensor is settled rigidly to the tracked target, and the field generator is set outside human body.

Fig. 2-6 A directional magnetic field sensor (left). A directional magnetic field sensor was inserted rigidly into the tracked target (right) [6].

Because the strength of induced magnetic field is small enough, it is safely to pass through human tissue. Accordingly, the electromagnetic tracking technology is convenient for intracorporeal tracking work. Compared with robot kinematics, this technology can be used to localize flexible endoscopic instruments such as flexible ultrasound transducers. The main issue is ferromagnetic interference. The system would be interfered by ferromagnetic material, such as metals, computers, OR tables, surgical instruments and internal signal interference. Even if many groups are dedicated to reduce the tracking errors, it still has no satisfactory enough outcome.

2.2.2 Optical Tracking Using Stereo Endoscope

With the increase of use of stereo endoscope in minimally invasive surgery, especially in recent years, optical tracking technology using stereo endoscope was proposed. In 2007, Gerard proposed a mixed-reality simulation of minimally invasive surgeries [5]. The main purpose is to help train surgeons. The instrument tracking technology used in Gerard's system is intracorporeal optical tracking using stereo endoscope. In 2014, Speidel et al. proposed a markerless 3D tracking technology used to track different da Vinci instruments [26].

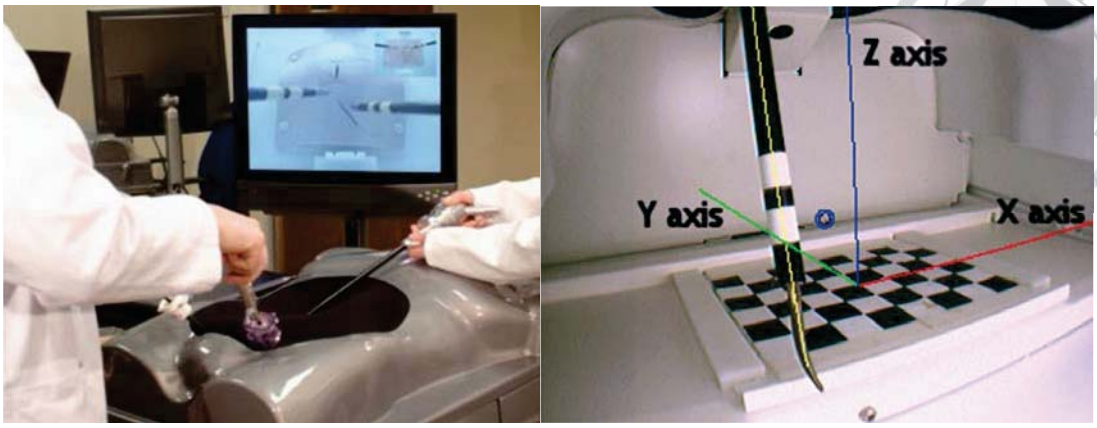

Fig. 2-7 Tracking technology Gerard's group proposed. Because they used stereo endoscope, once they found the tip position of instrument in 2D image, the depth information could be derived from relative position in stereo image [5].

In case that a stereo endoscope is used to replace traditional 2D endoscope, it means the depth information of each dot in the displayed image can be derived from stereo endoscope. Thus, the 3D tracking work is simplified as tracking tip of instrument in the 2D image. Once the 2D position of instrument tip is found, the depth information is derived in the meantime. And the coordinate of the instrument tip can be calculated. Using endoscope coordinate system as world coordinate system makes this technology need no other transformations, which makes the calibration simpler and reduces errors generated in transformation process.

This technology has advantages including simpler calibration process and less transformation errors. However, the largest limitation is that stereo endoscopes are not applied very popularly by hospitals due to the high expense. But it is still a potential

technology if stereo endoscopes are spread in the future.

2.2.3 Optical Tracking Using 2D Endoscope

Because general endoscopes using in minimally invasive surgery are still 2D endoscope, and to conquer the inconvenience of operation and inaccuracy problem occurred in technologies introduced above, we proposed an intracorporeal optical tracking system using 2D endoscope in 2013 [7].

Markers are affixed to marker modules fixed on instruments, directly using endoscope as image capture device to detect the markers and estimates positions and orientations of the instruments.

Advantages of this system are immune from ferromagnetic interference and achieve high tracking accuracy. The details of system structure and algorithms are introduced in Chapter 3.

2.3 Comparison and Summary

All the tracking technologies discussed above have some advantages and some disadvantages. Robot kinematics is most expensive compared with others. Errors of robot kinematics are enlarged when values of encoders are distorted by forces applied to a surface or the trocars. Though extracorporeal optical tracking provides an acceptable accuracy, it is also expensive due to the need of multiple cameras to solve visibility problem. Another disadvantage is operation interference due to the marker modules

settled on instruments. Electromagnetic tracking has no visibility problem, operation interference and it is relatively cheaper. However, the dominant problem is ferromagnetic interference. The error of electromagnetic tracking increases from 0.3 mm to 2.3 mm in environment within ferromagnetic interference. Intracorporeal optical tracking provides a good accuracy and has no ferromagnetic interference problem. The disadvantage of it is visibility problem. Intracorporeal optical tracking proposed in [7] uses square markers and rectangular marker modules, which may lead to unnecessary damages when touching tissues. This work applied intracorporeal optical tracking and uses cylindrical markers to reduce possibilities of accidental damages and to remain advantages of intracorporeal optical tracking.

Table 2-1 Comparison of tracking technologies

Sensor placement	Extracorporeal tracking		Intracorporeal tracking	
Approach	Robot kinematics 2005 J. Leven [12]	Optical tracking 2008 M. Feuerstein [3]	Electromagnetic tracking 2011 C. T. Yeo [25]	Optical tracking 2013 M. C. Ke [7]
Mean error	2.2 mm	2.6 mm	2.3 mm	1.1 mm
Ferromagnetic interference	No	No	Yes	No
Visibility problem	No	Yes	No	Yes
Operation interference	Yes	Yes	No	No
Damages to tissues	No	No	No	Yes
Cost (USD)	Millions	Tens of thousands	Tens of thousands	Hundreds

Chapter 3 Square Marker Optical Tracking

The main work in this research is to create an intracorporeal optical tracking system using cylindrical marker for minimally invasive surgery. In this chapter, an intracorporeal optical tracking system using square marker [7], which is proposed by our group in 2013, is introduced. It is based on Kato's ARToolkit [1]. In this research, the shape of marker is improved from square to cylinder. Hence, pattern and functions of square marker and the tracking algorithm of optical tracking system using square marker should be introduced before introduction of our design of cylindrical marker.

The system overview will be introduced in section 3.1, including the setting of devices and the flow of optical tracking. In section 3.2, the typical square marker will be introduced, including the pattern and functions of each part of square marker. The main tracking algorithm will be introduced in section 3.3. And in the end of this chapter, section 3.4, we summarize which functions should be existed in our cylindrical marker so that the proposed system can use the tracking algorithm of original optical tracking system.

3.1 System Overview

Ke et al. (our group) proposed an intracorporeal optical tracking system at 2013 [7]. An endoscope is adopted as the role of image capture device like camera in general optical tracking system, providing the raw image inside the surgical site. A rectangular marker

module is attached to the tracked instrument, and the distance between the marker module and the tip of the instrument is known by measurement in advance. Square markers, which is introduced in section 3.2, are affixed to the marker module. The system architecture including endoscope, tracked instrument within square markers is shown in Fig. 3-1. Marker detection and coordinate transformation from marker coordinates to endoscope coordinates is executed by Kato's ARToolkit [1].

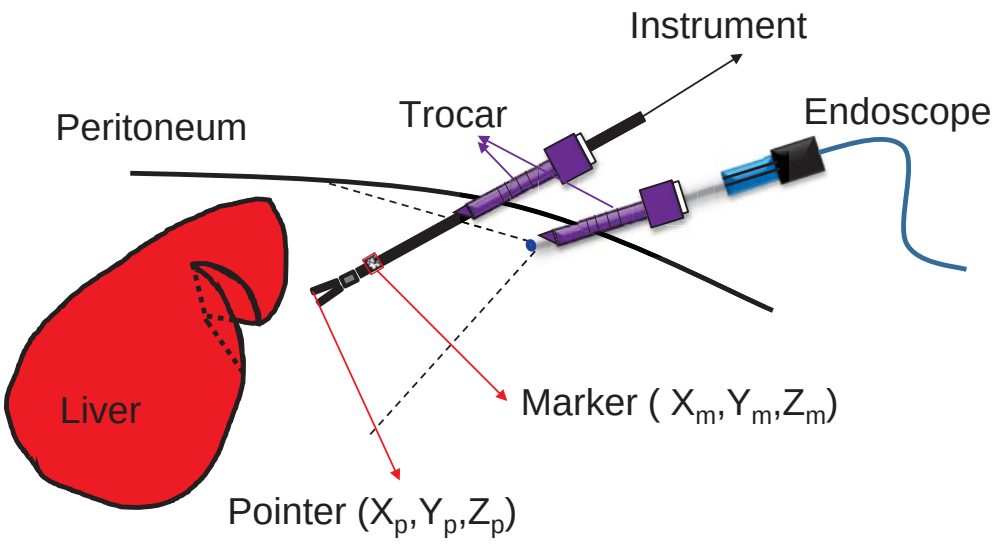

Fig. 3-1 Architecture of intracorporeal optical tracking using square marker [7].

Compared with extracorporeal optical tracking system, the intracorporeal optical tracking system we proposed has many advantages. Applying endoscope as image capture device shortens the distance between objects and image capture device, which reduces the incision of occlusion, enhances the tracking accuracy and reduces the cost. And less operation interference occurs.

The flowchart of intracorporeal optical tracking is shown in Fig. 3-2. Camera

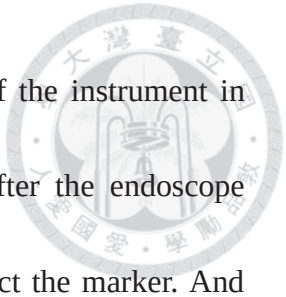

calibration and measurement of positions of markers and the tip of the instrument in marker coordinate system is completed as off-line procedures. After the endoscope capture images, a sequence of image processing is operated to detect the marker. And then the transformation matrix from marker coordinates to endoscope coordinates is calculated using the information of detected marker, distortion parameters as well as intrinsic parameters derived from off-line camera calibration, and marker potions in marker coordinate system. The position in camera coordinate system can be derived by transforming the position in marker coordinate system using extrinsic parameter matrix. The position in camera screen coordinate system can be derived by transforming the position in camera coordinate system using intrinsic parameter matrix. The tracking work is achieved. The detail algorithm is introduced in section 3.3.

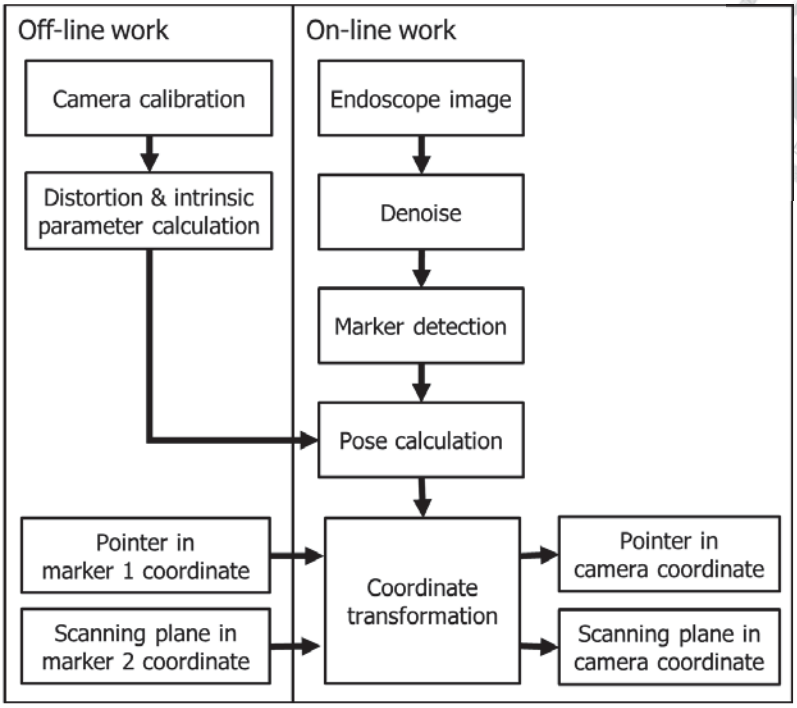

Fig. 3-2 The flowchart of intracorporeal optical tracking using square marker [7].

The world coordinate system here is endoscope coordinate system, different from general optical tracking system. Since the relative distance between organism and instruments is more important for surgeons in clinical minimally invasive surgery, and the useful information would be projected to endoscope image by augmented reality, it can be applied using endoscope coordinate system as world coordinate system. The advantage is to reduce the procedures of coordinate transformation from many times to single one so as to reduce the errors generated from multiple coordinate transformations.

3.2 Square Marker

The typical marker used in ARToolkit is a square marker as Fig. 3-3.

Fig. 3-3 Single square marker [1].

A square marker should provide some information to the calculation of transformation matrix. Four corner points is used to calculate the transformation matrix form marker coordinates to camera coordinates by the relation of positions of four corner points in marker coordinate system and which in camera screen coordinate system. A marker direction is used to determine the relationship between corner points detected from marker detection and corner points in marker coordinate system. In other words, it's used to differentiate which direction the marker is from four possible situations. If there are many markers in the surrounding, some information should be provided to differentiate different markers. Due to these requirements, the square marker is designed to have some characteristics for marker detection shown as bellow. The illustration is shown in Fig. 3-4.

1. Vacant space around the marker
2. Square
3. Planar surface
4. A pattern inside

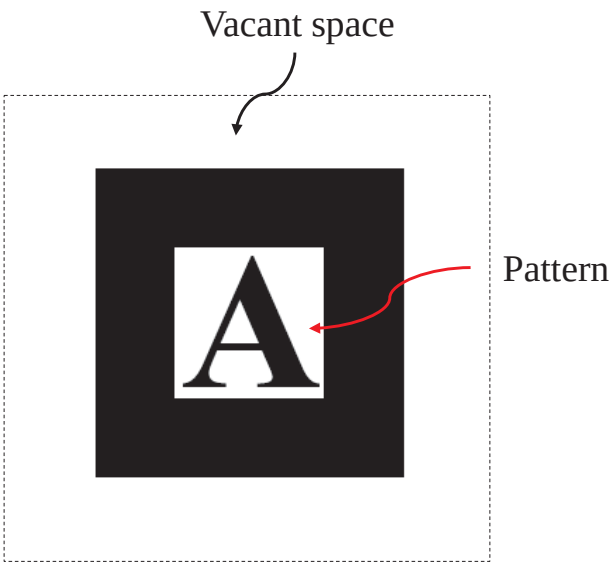

Fig. 3-4 Typical square marker has vacant space and pattern inside.

Vacant space is used for the convenience of marker detection. The marker body is separated from the surrounding by the vacant space, which makes the marker body is obvious in the image. A square design is used because there are four corner points in a square, which is one of requirements for marker detection: providing four corner points. A planar surface makes sure that the four lines of the marker contour in image are still straight lines. Ideally, a straight line looks like a straight line in the image no matter observing it from any view angle. That's important for the marker detection because a line fitting algorithm can be used to obtain the four straight lines and then the corner points of the marker are derived by calculating the intersections of the four straight lines. The pattern inside can be designed as many different styles, like numbers, simple pictures and so on, a limitation is it needs to have direction difference. It is used for marker

detection to differentiate the marker id from multiple markers and to determine the marker direction.

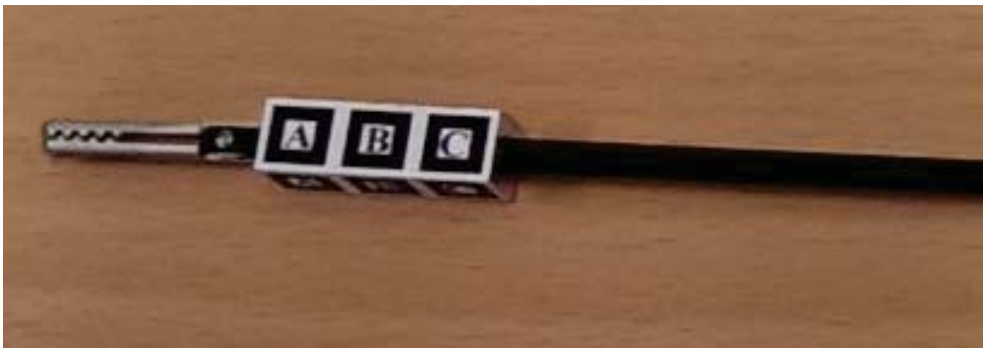

Fig. 3-5 Square markers are affixed to the marker module attached to the tracked instrument. Four sides to make sure view-invariant and multiple marker [7].

We apply multiple markers as a marker set and affix it to the marker module, shown in Fig. 3-5. Each three markers in one side of the marker module is used to enhance the tracking accuracy because an iteration process is used in the algorithm of calculating transformation matrix. The other advantage is that if some markers are occluded or stained by blood, the system can still achieve the tracking work as long as at least one marker of them is visible. Four sides of the marker module make sure view-invariant. In other words, after rotation, the marker set will still visible. The only difference is maybe the side of marker set observed in this frame is different from which in last frame.

3.3 Tracking Algorithm

The tracking algorithm used here is Kato's approach [1]. Sufficient accuracy and fast

processing speed are advantages of Kato's approach.

The main purpose is to obtain the transformation matrix from marker coordinates to camera coordinates (T_{cm}) using a size-known marker, so that the transformation matrix can be used to derive each point in camera coordinate system from their coordinates in marker coordinate system. (3.1) shows the transformation from marker coordinates to camera coordinates. The relationship between marker coordinates and camera coordinates is shown in Fig. 3-6.

$$\begin{bmatrix} X_c \\ Y_c \\ Z_c \\ 1 \end{bmatrix} = \begin{bmatrix} V_{11} & V_{12} & V_{13} & W_x \\ V_{21} & V_{22} & V_{23} & W_y \\ V_{31} & V_{32} & V_{33} & W_z \\ 0 & 0 & 0 & 1 \end{bmatrix} \begin{bmatrix} X_m \\ Y_m \\ Z_m \\ 1 \end{bmatrix} = \begin{bmatrix} V_{3\times3} & W_{3\times1} \\ 0 \quad 0 \quad 0 & 1 \end{bmatrix} \begin{bmatrix} X_m \\ Y_m \\ Z_m \\ 1 \end{bmatrix} = T_{cm} \begin{bmatrix} X_m \\ Y_m \\ Z_m \\ 1 \end{bmatrix} \tag{3.1}$$

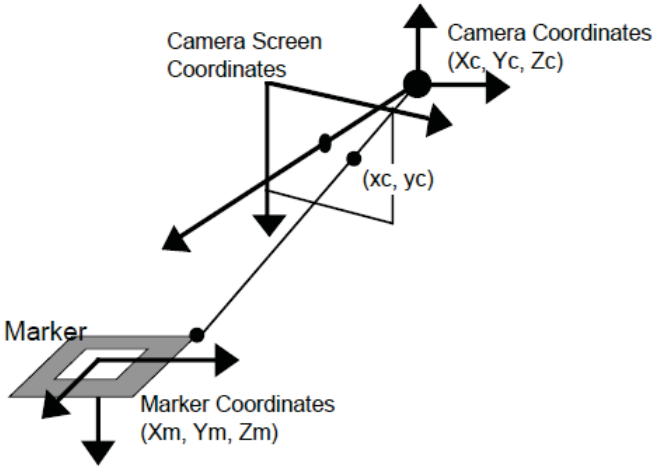

Fig. 3-6 The relationship between marker coordinates, camera coordinates and camera screen coordinates [1].

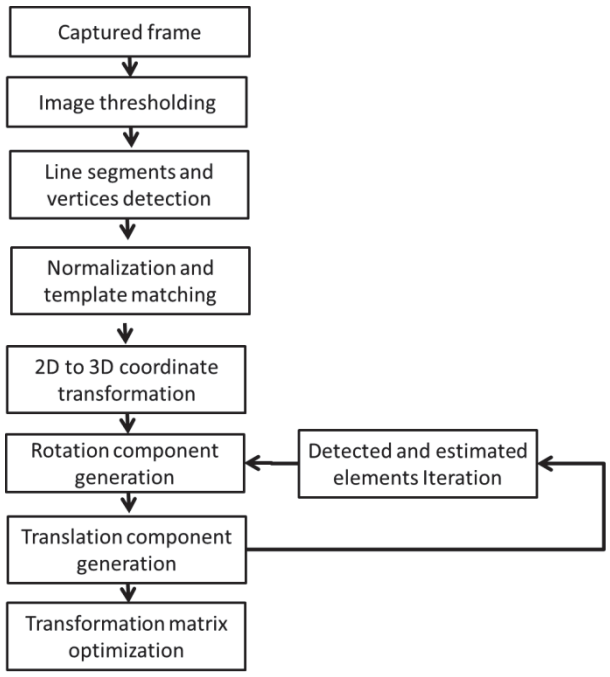

Fig. 3-7 The flowchart of Kato's tracking approach [1].

After capturing the image, first step is generating a binary image by image thresholding. The second step is to find contours from the binary image by gradient difference. Lager contours are regarded as potential marker regions. Then the four lines of potential marker regions are simply extracted by fitting line segments to the marker regions. And the four vertices are found by intersecting the four lines. All parameters of the four vertices and the four lines found from potential marker regions are stored for later processes.

The sub-image within regions of potential markers are normalized, warped to squares and then compared by template matching with patterns which were given the system off-line to identify specific marker name (marker id). The normalization process

uses a perspective transformation shown in (3.2). All variables in the matrix in (3.2) can be determined by substituting camera screen coordinates and marker coordinates of the detected markers for (x_c, y_c) and (X_m, Y_m) respectively.

$$\begin{bmatrix} hx_c \\ hy_c \\ h \end{bmatrix} = \begin{bmatrix} N_{11} & N_{12} & N_{13} \\ N_{21} & N_{22} & N_{23} \\ N_{31} & N_{32} & 1 \end{bmatrix} \begin{bmatrix} X_m \\ Y_m \\ 1 \end{bmatrix} \tag{3.2}$$

Two parallel sides of detected square markers can be projected on the images. The equations of lines can be represented as (3.3). The values of these markers has been obtained in the line fitting process in advance.

$$a_1 x + b_1 y + c_1 = 0, \quad a_2 x + b_2 y + c_2 = 0 \tag{3.3}$$

$$P = \begin{bmatrix} P_{11} & P_{12} & P_{13} & 0 \\ 0 & P_{22} & P_{23} & 0 \\ 0 & 0 & 1 & 0 \\ 0 & 0 & 0 & 1 \end{bmatrix}, \quad \begin{bmatrix} hx_c \\ hy_c \\ h \\ 1 \end{bmatrix} = P \begin{bmatrix} X_c \\ Y_c \\ Z_c \\ 1 \end{bmatrix} \tag{3.4}$$

The perspective projection matrix from camera coordinates to screen coordinates obtained from camera calibration is shown in (3.4). By substituting x_c and y_c in (3.4) for x and y in (3.3), the two parallel sides whose equations are shown in (3.3) can be represented as (3.5) in the camera coordinate system.

$$\begin{aligned} a_1 P_{11} X_c + (a_1 P_{12} + b_1 P_{22}) Y_c + (a_1 P_{13} + b_1 P_{23} + c_1) Z_c = 0 \\ a_2 P_{11} X_c + (a_2 P_{12} + b_2 P_{22}) Y_c + (a_2 P_{13} + b_2 P_{23} + c_2) Z_c = 0 \end{aligned} \tag{3.5}$$

The direction vector of the two parallel sides can be derived by the outer product $n_1 \times n_2$, where n_1 and n_2 are normal vectors of the planes shown in (3.5). Given that

u_1 and u_2 are two unit direction vectors of square marker, they should be perpendicular ideally. But they are not due to image processing errors. It's necessary to refine the direction vectors form u_1 and u_2 to v_1 and v_2, shown in Fig. 3-3. And then calculate the third unit direction vector v_3 form outer product $v_1 \times v_2$. Here, by concept from linear algebra the rotation component $V_{3\times3}$ in the transformation matrix T_{cm} from marker coordinates to camera coordinates specified in (3.1) is $\begin{bmatrix} v_1^t & v_2^t & v_3^t \end{bmatrix}$.

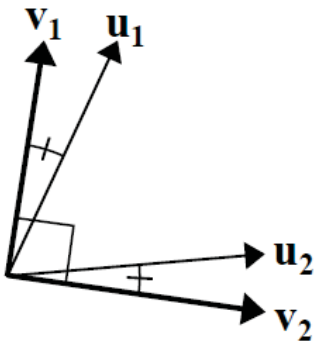

Fig. 3-8 u_1 and u_2 are used to calculate refined perpendicular unit direction vectors v_1 and v_2.

Using (3.1) and (3.4), the four vertices coordinates of the detected marker in the marker coordinate system and those coordinates in the camera screen coordinate system, eight equations totally, the translation component $W_x W_y W_z$ are generated by solving these equations.

Here, the transformation matrix from marker coordinates to camera coordinates is obtained. And then the transformation matrix is optimized by minimize the sum of

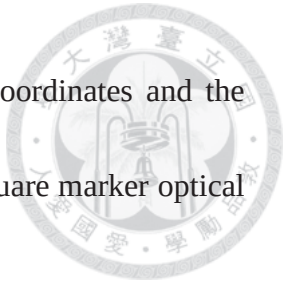

difference between transformed camera coordinates form marker coordinates and the detected coordinates. This is the main tracking algorithm used for square marker optical tracking.

3.4 Summary

The tracking system applied in this research is based on the optical tracking system using square marker introduced in this chapter. Differences between the new proposed system and the original system using square marker are the change of marker shape from square to cylinder and the algorithm of marker detection. Algorithm of calculating transformation matrix of the original system is still used in the new proposed system.

From the introduction in this chapter, we can see what are needed for the system to calculate a transformation matrix from marker coordinates to camera coordinates are four corner points, direction and marker id. Thus, if there is a new design of marker which is expectedly used in original optical tracking system, the new marker also has to provide four corner points, direction and marker id. Consequently, the cylindrical marker which will be introduced in Chapter 4 is designed with ability to provide these information.

Chapter 4 Cylindrical Marker Optical Tracking

This chapter presents system architecture of intracorporeal optical tracking using cylindrical marker. Different from square marker optical tracking, the markers used in this work are cylindrical markers which are affixed to cylindrical marker modules. The cylindrical marker is a marker set within many independent markers. The design of marker pattern is one of main contributions of this work. The tracking procedures can be simply classified into two: marker detection and coordinate transformation. To achieve tracking work using cylindrical marker, it's necessary to build some specific algorithm to detect cylindrical markers and to extract features of them. The method to calculate transformation matrix is the same with method discussed in section 3.3. Hence, after extracting features of cylindrical markers, the following work is the same with system introduced in chapter 3.

The system architecture and abstract ideas are introduced in section 4.1. The design of cylindrical marker module is introduced in section 4.2. The particular pattern design is introduced in section 4.3. The algorithm to detect cylindrical markers and to extract features of them is introduced in section 4.4. Because the cylindrical marker is a marker set within many independent markers, the interactions between independent markers are introduced in section 4.5.

4.1 System Overview

In the field of hardware, the main difference between optical tracking using square marker and optical tracking using cylindrical marker is the marker module. The architecture is shown in Fig. 4-1. Because the marker module is designed as a cylinder, it can avoid damages to tissues when touching tissues in surgeries. To achieve tracking work using cylindrical marker module, the design of marker pattern is very important. It's one of the main contributions of this work.

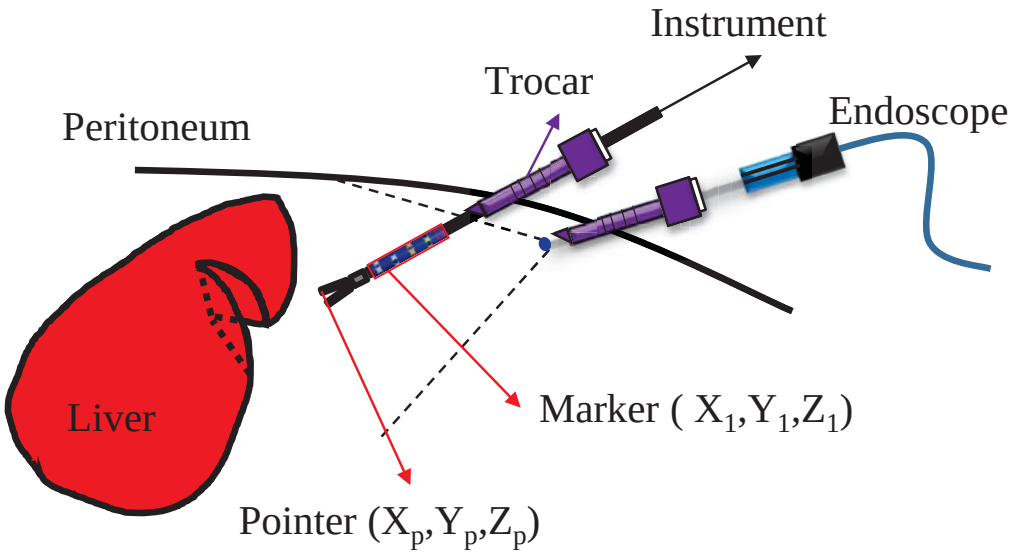

Fig. 4-1 Architecture of intracorporeal optical tracking using cylindrical marker.

In the field of algorithm, Fig. 4-2 shows the flowchart of intracorporeal optical tracking using cylindrical marker. When image capture device, endoscope here, captures an image, the system detects cylindrical markers and extracts features of them. After deciding which markers are confident, their features are used to calculate transformation

matrix from marker coordinates to camera coordinates, which is extrinsic parameter matrix. The intrinsic parameter matrix are derived off-line. The position in camera coordinate system can be derived by transforming the position in marker coordinate system using extrinsic parameter matrix. The position in camera screen coordinate system can be derived by transforming the position in camera coordinate system using intrinsic parameter matrix. After that, the tracking work is achieved.

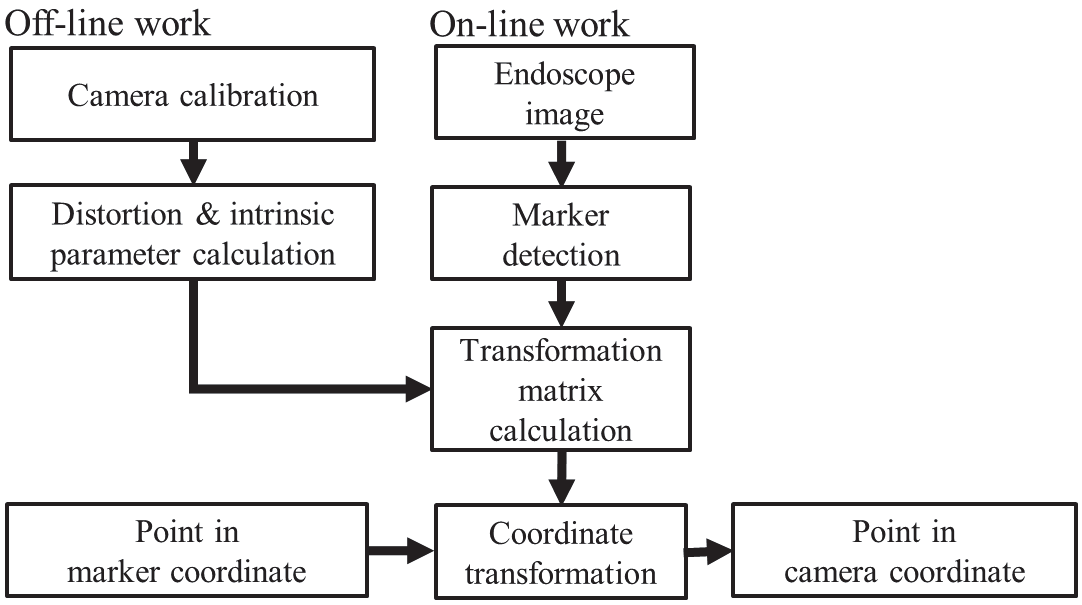

Fig. 4-2 Overall flowchart of intracorporeal optical tracking using cylindrical marker.

4.2 Cylindrical Marker Module

Adoption of cylindrical marker module and cylindrical marker is the largest difference for this work comparing with intracorporeal optical tracking system using

square marker. Because the instruments are used inside human body, the existence of square marker module may give rise to unnecessary damage to tissues by touching and mowing it accidentally.

The reason why don't affix marker to instrument surface directly is that we can't promise the instrument is a perfect cylinder. The tracking accuracy may be reduced by imperfect instrument surface. This issue can be solved when using a specific marker module manufactured precisely. Of course, the aim of this work is to print marker directly on the instrument surface without marker module when instruments are manufactured in the future.

The marker module is designed as a cylinder within 6.8 mm diameter, which ensures the instruments within this marker module can penetrate trocars within 7 mm diameter, and the length of it is 40 mm. The distance between marker module and tip of instrument is 25 mm. The design illustration is shown in Fig. 4-3. A punctured line is used to make sure markers are affixed precisely to the marker module by aligning markers and the punctured line. Fig. 4-4 shows the picture of it.

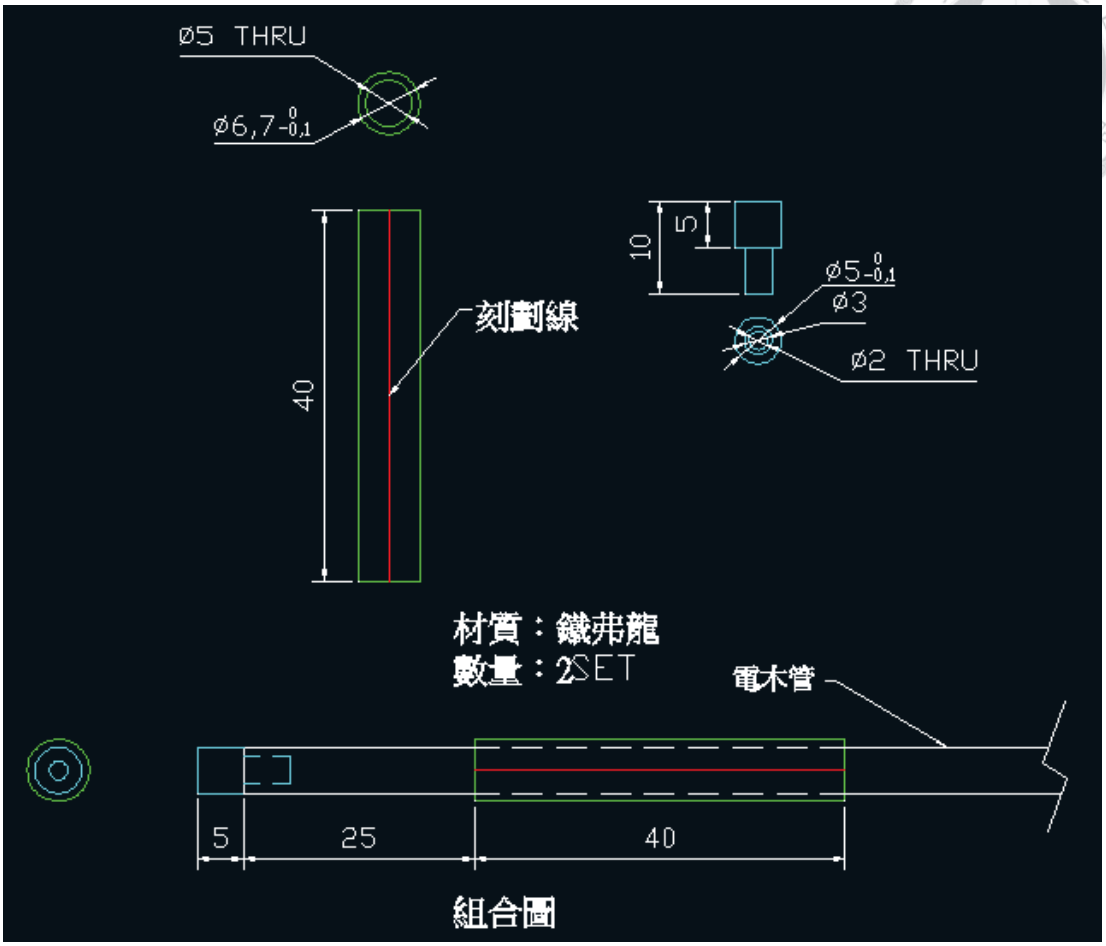

Fig. 4-3 Design illustration of cylindrical marker module.

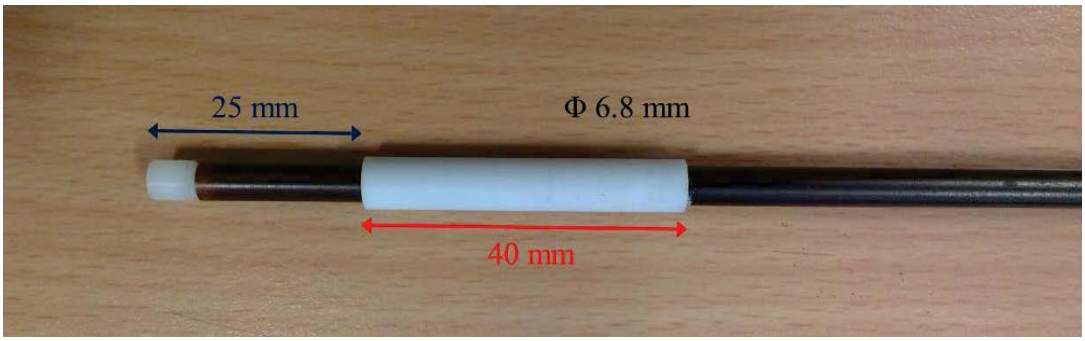

Fig. 4-4 Cylindrical marker module, no marker affixed to it.

4.3 Pattern Design

Pattern design of cylindrical marker is a key point of this work. The pattern is

designed with specific features responding to which in square marker. After marker detection, features can be extracted and can be used in transformation matrix calculation. The illustration of complete marker set is shown in Fig. 4-5, and a marker set is affixed to a marker module like Fig. 4-6. Single marker is introduced in this section, and the multi-layer marker set is introduced in section 4.5.

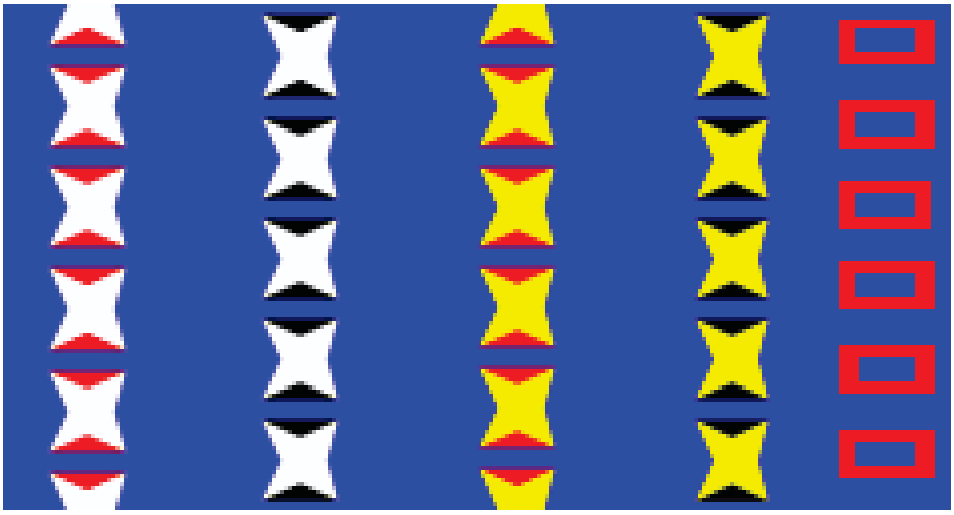

Fig. 4-5　Complete designed cylindrical marker.

Fig. 4-6　Complete cylindrical marker set is affixed to a marker module attached to instrument.

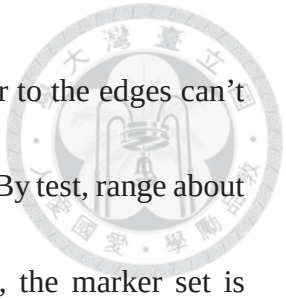

Because the edges of a cylinder are condensed, information near to the edges can't be extracted easily and accurately, which leads to loss of information. By test, range about 120 degrees of a cylinder can be observed more completely. Thus, the marker set is designed with many single markers, making sure that some markers not near to edges of cylinder can be observed from any view angle. The marker set has four layers of markers. The selection of number of markers contained in a layer and each marker's size are trade-off problems. Larger marker size can make the observed marker have more pixels, which can provide more information to enhance the accuracy of marker detection. Nevertheless, it reduces the number of markers in each layer. By test, five markers a layer can let some markers observed no matter from any angle and keep each marker large enough. And a shift of half of marker length exists between each two layers. The hollow rectangles, called direction rectangles, in the right of marker set shown in Fig. 4-6 are used to identify marker direction.

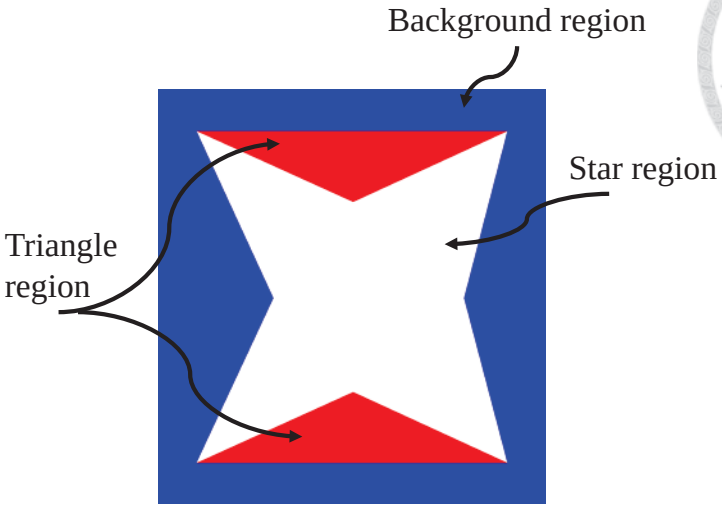

Fig. 4-7 Pattern of cylindrical marker, including background region, star region and triangle region.

The designed pattern of a single marker is composed of three parts, including background region, star region and triangle region, shown in Fig. 4-7. The background region is used to segment marker set from image more easily. Hence, the color of background region is selected differentiable enough from reddish background. In the meanwhile, colors of other regions are also selected differentiable enough from background region, so that the possibility of misdetection is reduced.

The star region has two functions: offering corner points and marker identification. The star region is designed with four convex acute angles, which are detected by corner detection introduced in 4.4.3 and provided for transformation matrix calculation. Color of star region is an index for marker identification like colors of other regions.

Two triangle regions of a marker have two functions. The first is specific color as

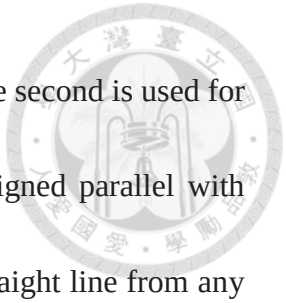

combination with colors of other region for marker identification. The second is used for precise corner detection. The longer side of a triangle region is aligned parallel with instrument, making sure that the longer side can be observed as a straight line from any view angle no matter how instruments are rotated. This is a key point for precise corner detection.

4.4 Marker Detection Algorithm

It is necessary providing features of markers for transformation matrix calculation. The necessary features are discussed in 3.4, including four corner points, direction and marker id. The purpose of marker detection is to exact features of designed cylindrical markers.

Fig. 4-8 shows the flowchart of marker detection. When capturing an image from image capture device, the first thing is to find potential marker sets. Color segmentation is used to segment specific colors, which are designed in marker sets, from reddish background of surgical image. Contours are used to detect whether the segmented regions are markers. If contours of the segmented regions have inlayer contours, the regions may be potential marker sets. And then marker id of each markers of the marker set is determined by the combinations of colors of each regions. The corner points are extracted in two stages. The first is rough corner detection. Corner points extracted using rough corner detection are used in marker direction and precise corner detection. The marker

direction are determined using relative positions of each marker and the background region, or determined using direction rectangle. Finally, precise corner points are extracted. To here, all the features for transformation matrix calculation are extracted. The detailed algorithms are introduced in the following sections.

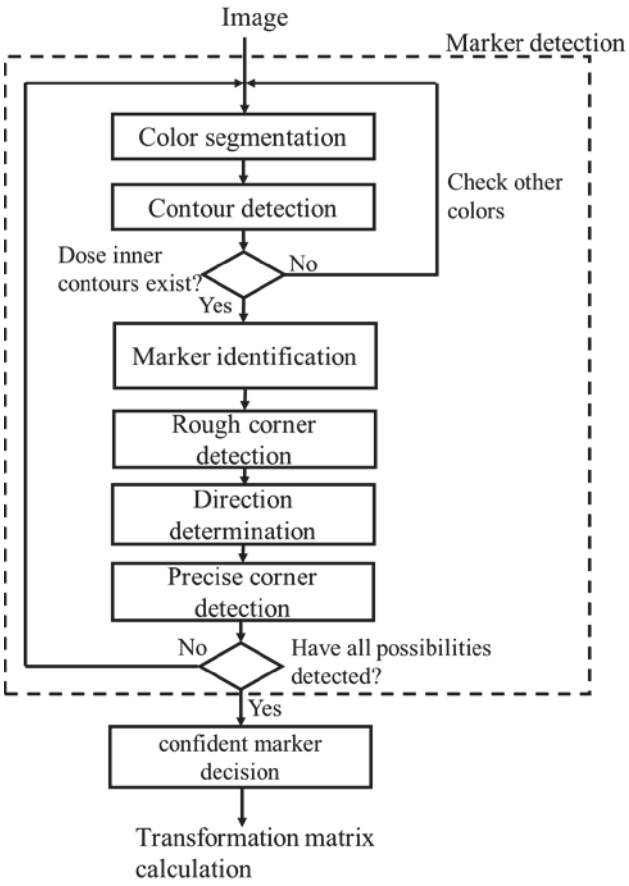

Fig. 4-8 Overall flowchart of marker detection for cylindrical marker.

4.4.1 Color Segmentation

The first stage of marker detection is to find potential markers. A general thought is to detect potential parts from image by visual cues [26]. Different visual cues are tested for finding which are useful for this task.

HSV Color Cue

An original surgical image is separated into three channels, hue, saturation and value. The hue channel is influenced by strength of light and the marker color in RGB space. The hue value will be enlarged if the strength of light is enhanced, and vice versa. If a region in image is reflective, the hue value of it will be very high. On the other hand, if the color of region is brighter in RGB space, like white, yellow and so forth, the hue value of it is also higher.

The saturation channel and value channel are not distinguishable as hue channel in surgical image.

Gray Color Cue

Due to the influence of light strength, strength of a dot in gray space varies frequently. If a dot in image is lighted, the strength of it in gray space will be high even it’s a deep color such as black. Thus, gray color cue is thought not a great cue for detecting markers inside human body.

RGB Color Cue

Color cue in RGB space is more distinguished compared with other color cue, for the predominant reddish background inside human body. The common colors appeared in a surgical image are red, white, black and yellow. Green and blue are rare. That means the marker can be design as blue or green, and it can be distinguished simply from a

reddish background.

More importantly, even a dot is lighted and it becomes brighter, it still remain primitive RGB color information. For example, when a blue dot whose blue intensity is larger than the other two is lighted, its blue intensity remains larger than the other two, even its green intensity and red intensity are enhanced.

Algorithm of Color Segmentation

A dot in an image has three channels, red channel, green channel and blue channel. For the convenience of color segmentation, intensities of adopted colors in marker are not high but low, no middle. The reason is to reduce the illumination variance. For example, intensities of blue are $(\text{Low}, \text{High}, \text{Low})$. Intensities of red are $(\text{High}, \text{Low}, \text{Low})$.

By comparing the differences of intensities of channels and the value of intensities, different colors can be differentiated. For instance, if intensities of three channels are all high, color of the dot is identified as white. If intensity of blue channel is high and intensities of the other two channels are low, the dot is identified as blue. By the process, dots with specific color in an image can be segmented.

When a source image is provided, the first thing of marker detection is to segment the potential markers by segmenting specific color which is the same with marker background region. After that a binary image, intensities of dots with segmented color is set as highest and intensities of dots without segmented color is set as zero, is generated.

After that, an ROI is set larger than the segmented potential marker. For the need of detecting different regions of a marker, color segmentation is used in the ROI of image.

Color Compensation

A special phenomenon of color mixture occurs when detecting specific color from an original image. There are some yellow star regions in original image like the left of Fig. 4-9. When segmenting yellow part from it, the segmented yellow star regions are not pretty complete, like the right of Fig. 4-9. If seeing in detail, a phenomenon can be discovered is that some part of the yellow star regions near the contour are not be segmented as yellow parts, but they are segmented as white parts, shown in the center of Fig. 4-9. The reason is specified as follows.

Intensities of RGB channels of yellow is $(\text{High}, \text{High}, \text{Low})$. Intensities of RGB channels of white is $(\text{High}, \text{High}, \text{High})$. Intensities of RGB channels of blue is $(\text{Low}, \text{Low}, \text{High})$. However, on the boundary between yellow star and blue marker background, the B channel of some dots which should be segmented as yellow is enhanced due to mixture with near blue dots, which caused the dots are segmented as white dots$(\text{High}, \text{High}, \text{High})$. Similar case occurs on the boundary between yellow stars and the black regions. Thus, a color compensation is needed to compensate the outcome of yellow compensation. When observing some yellow regions in the image, we can take the union of segmented yellow image and segmented white image as a new segmented

yellow image. This method can be adopted for other color mixture case.

Fig. 4-9 An example showing color mixture. Original image (left). Detected white part of the original image (center). Detected yellow part of the original image (right).

4.4.2 Contour Detection

Contours of potential markers are used for many application, containing judging whether the potential marker is a real marker and corner detection. General contour detection uses gradient information to detect contours. Dots on contours have larger gradient than other dots with plainer gradient. How to decide the threshold of gradient is a main problem in general image. Unnecessary contour segments are detected when using a lower threshold of gradient, and it loses some contours when using higher threshold of gradient. In our case, the problem doesn't exist. The source image in our case, shown in Fig. 4-10, is a binary image. The intensities of dots are not highest but lowest. Thus, dots on a contour have high gradient value and gradients of other dots are zero. Contours can be detected definitely using gradient information without threshold problem. The problem is how to determine which contours are contours of potential markers.

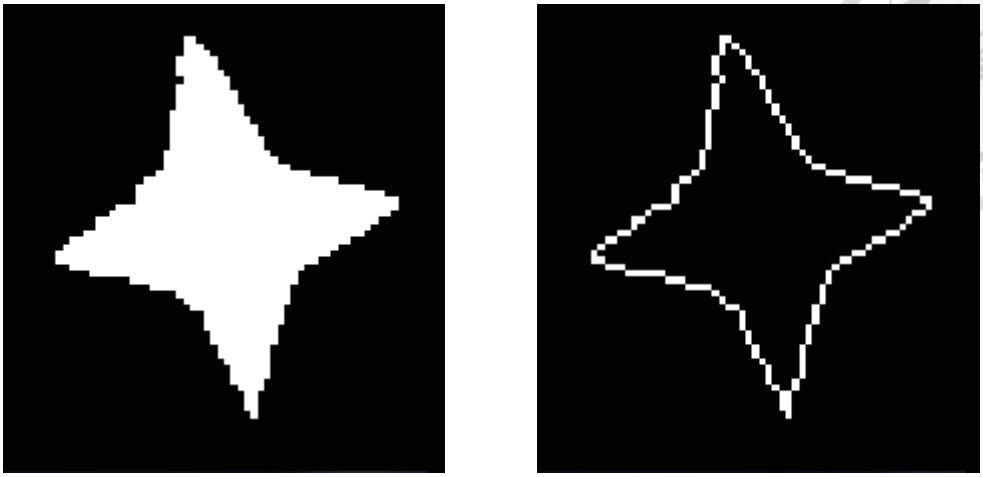

Fig. 4-10 Original binary image (left). Contour image (right).

In this work, marker pattern is designed with several regions with different colors. After color segmentation using color of background region, it is observed that the region of marker set in binary image has hollow caves responding to other regions in background region. Accordingly, the detected contours of background region have inlayer contours. Other detected contours, which are not responding to background region of marker set, don’t exist inlayer contour in general case, which is a useful information for filtering possible marker set. In other words, if the detected contour exists no inlayer contour, the contour is not a contour of background region of a marker set.

4.4.3 Rough Corner Detection

The method to detect corner points of cylindrical marker is designed as a two stage algorithm. First stage of it is rough corner detection, and the second stage of it is precise corner detection which is introduced in 4.4.6.

After contour detection of specific color part of image, a contour image is obtained. If the specific color is one of designed marker background region color and there exist inlayer contours, the contour is recognized a potential background region of marker set, and the inlayer contours are recognized potential markers. Before marker identification, the rough corner points should be detected. The method to detect rough corner points is to enclose the inlayer contour with a rectangle within minimum area. Because instruments incline with some angles, the intersections of potential contours and the enclosed rectangle within minimum area are corner points of potential markers, shown in Fig. 4-11.

Due to illumination variance, the detected contours usually jitter, as the result, the detected rough corner points also jitter and not so precise. But they can be still used for some applications which only need rough corner points.

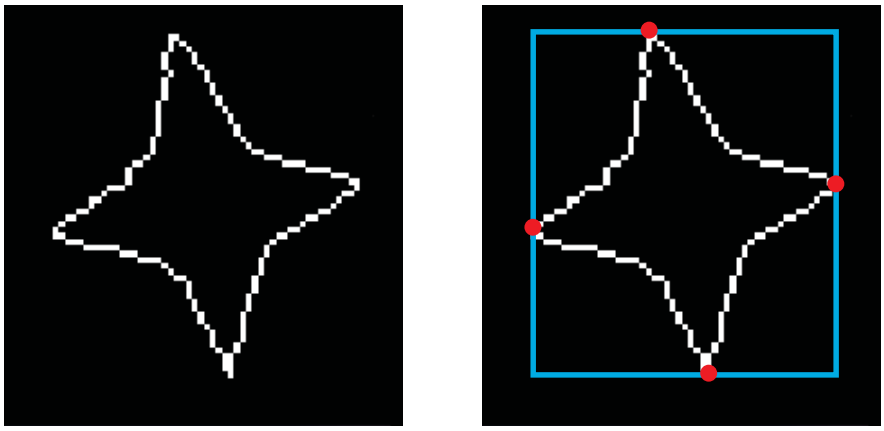

Fig. 4-11 Contour image (left). The contour are enclosed by a rectangle, and the intersections of the contour and the rectangle are corner points.

4.4.4 Marker Identification

The purpose of marker identification is to identify the detected marker name (marker id). A marker set has multiple layers, and each layer has multiple same markers. In marker detection process, multiple markers are detected. Marker name of each detected marker has to be identified correctly. Marker id is one of necessary information for transformation matrix calculation.

Markers in different layers has different color combinations. In Fig. 4-12, from left to right, color of star region of markers in the first layer and which of markers in the second layer are the same. Color of star region of markers in the third layer and which of markers in the fourth layer are the same. On the other hand, color of triangle region of markers in the first layer and which of markers in the third layer are the same. Color of triangle region of markers in the second layer is the same with which of markers in the fourth layer. There are three different color information for each detected maker.

Fig. 4-12 Illustration of a marker set affixed to instrument. Markers in different layers has different color combinations, which is the same when markers are in the same layer.

After marker set is detected using contour detection, inlayer contours within area larger than a threshold are supposed as markers. Center of a marker is derived by averaging the coordinates of four corner points of the marker. Star color of a marker is decided by color of center of the marker. The next thing is to search possible colors of triangle region in ROI of the detected marker. A color of triangle region of a marker is decided when meeting two conditions: there are two regions within specific color existing and their areas are both larger than a threshold.

To here, each independent marker has information of three colors, including which of background region, star region and triangle region. This is enough for system to identify markers, providing each marker for a marker number defined off-line.

4.4.5 Direction Determination

Each marker of marker set has four possible direction. It’s necessary to determine

marker direction. In this work, methods to determine marker direction have two: position relative to background region and direction rectangle.

Position Relative to Background Region

Enclose the detected background region of marker set with a minimum area rectangle, which is defined as background rectangle, shown in Fig. 4-13. The difference between longest side and shortest side of a background rectangle is obviously large. The major axis of background rectangle is derived using the four vertexes of background rectangle. Marker direction should be parallel with the major axis, so the possible marker directions of each marker can be reduced into two. Divide the major axis into two parts and calculate centers of mass of them. Take average of four coordinates of corner points of detected marker simply as center of mass of it. And then the center of mass is compared with two center of mass of divided major axis to know the marker is closer to which side of major axis. Because the marker id is known and which side the marker is closer to is known, the marker direction is derived. The prerequisite is the distances between each two marker layers should be designed large enough.

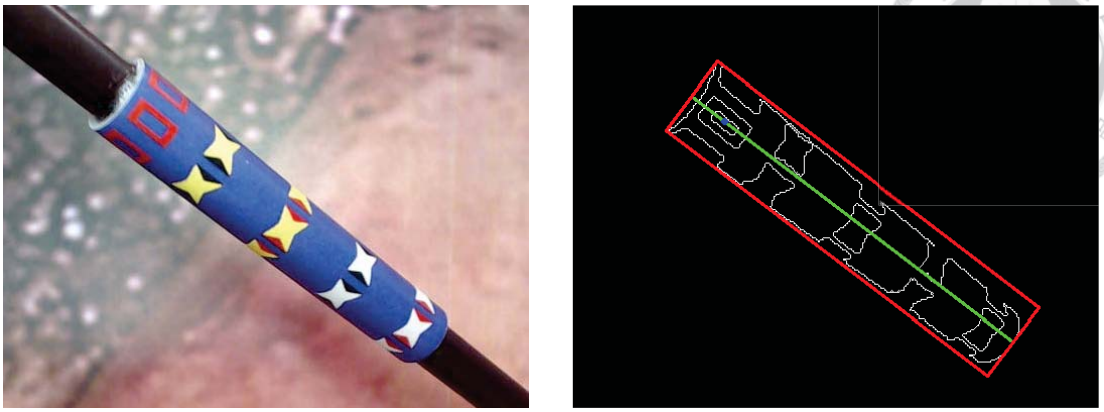

Fig. 4-13 RGB image of marker set (left). Blue contours of marker set (right). Red rectangle is the background rectangle of marker set. Green line is the major axis.

Direction Rectangle

The other method to determine marker direction is specified here. The hollow rectangles in the right of marker set shown in Fig. 4-14 are direction rectangles. There are two corner points closer to the direction rectangle for each independent marker, which is used to determine marker direction. First, calculate center of mass (C.M.) of direction rectangle and then project it to the major axis of marker set, called p_r^{proj}. Project four corner points of each marker to major axis of marker set, called p_i^{proj}, $i = 0,1,2,3$. Calculate the length differences between p_r^{proj} and each p_i^{proj}, called d_i, $i = 0,1,2,3$. The marker direction is determined by taking the largest and the second largest, because only one case exists.

Fig. 4-14 The hollow rectangles in the right of marker set are direction rectangles, which are used to determine marker direction.

These two method both can be used to determine marker direction, which means redundant. The reason why adopting the two methods is to avoid occlusions. When parts of marker set are occluded, the first method may determine an incorrect marker direction because of incomplete background rectangle. In the case, the second method is preferable. On the other hand, when direction rectangles are occluded, of course the second method cannot be used to determine a correct marker direction. The first method is adaptable in this case. Certainly, the two methods can both be used to determine correct marker direction if there are no occlusions.

4.4.6 Precise Corner Detection

Corner points are detected initially by rough corner detection. However, due to jittering of contour caused by illumination variance, corner points detected by rough corner detection are also jittering. This phenomenon increases errors of transformation

matrix. So it's necessary to refine the corner detection.

The idea of precise corner detection is intersecting straight lines to derive precise corner points, shown in Fig. 4-16. Lines parallel to instrument are observed as straight lines in image from every view angles, which can be used. Another lines used to derive intersections are straight lines fitted by contours between inner corners and outer corners.

Because corner points and marker direction are already derived in early stages, contours between which two corner points are parallel to instrument are known. The convex corner points detected in early stage are defined as outer corners, and the concave corners are defined as inner corners, shown in Fig. 4-15. The line parallel to instrument in image L_1 is fitted by least squares regression using contour between two outer corners. To reduce possibility of missing determination, the contour used to fit a line is pruned by reducing several points on two sides of it.

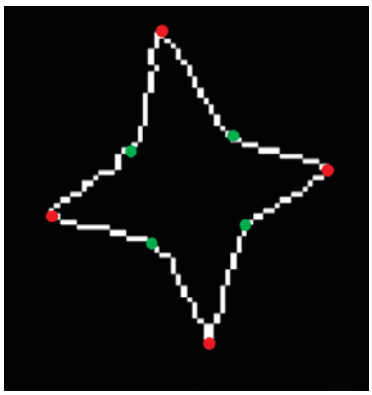

Fig. 4-15 Red points represent outer corner points of the contour. Green points represent inner corner points of the contour.

The prerequisite to derive another fitted line is inner corner points of the contour. Shown in lower left of Fig. 4-16, connect two outer corner points to build a line L_{in} and calculate distances d_i between L_{in} and every point of contours between the two outer corner points. The largest d_i means that the i_{th} point is the inner corner points. And, prune the contour between inner corner point and outer corner points by several points. The derived line L_2 is fitted by least squares regression using this pruned contour.

The points intersected by lines parallel to instrument L_1 and lines between inner corner points as well as outer corner points L_2 are new precise corner points. All the procedures are shown in Fig. 4-16. Different from rough corner detection, corner points detected using this method includes float information, which enhances precision. On the other hand, corner points detected using rough corner detection may be closer to center of marker than real position because of color mixture, but corner points detected by this method are not.

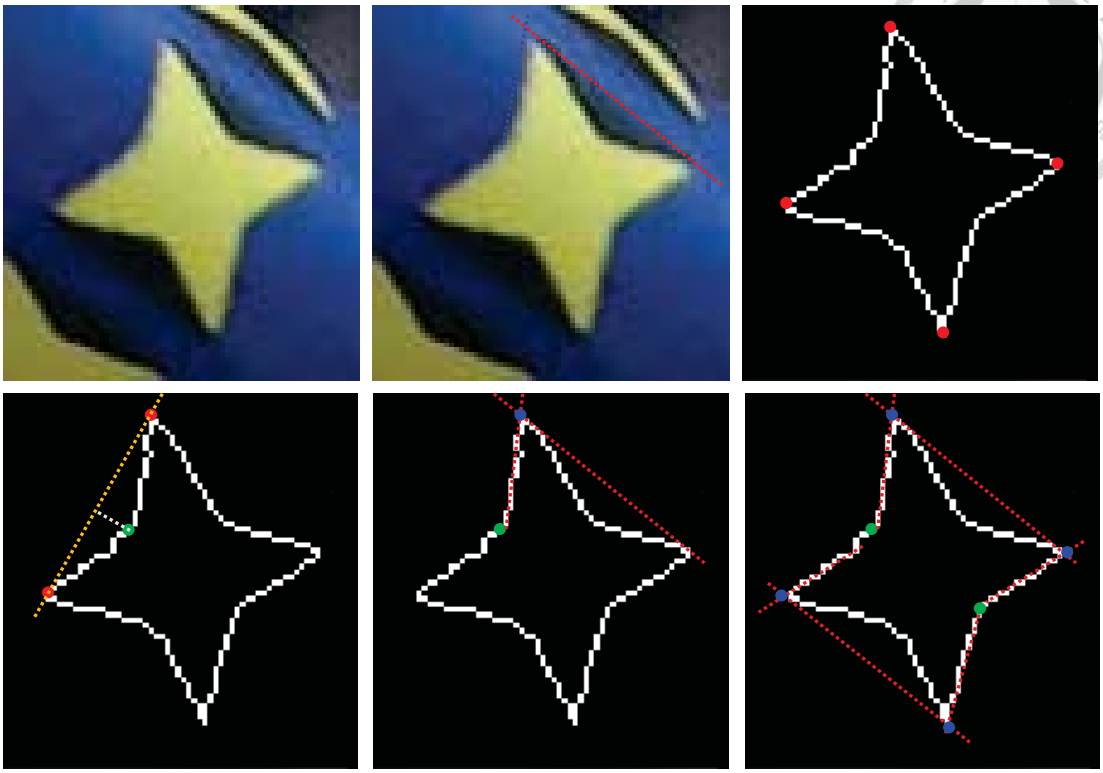

Fig. 4-16 ROI of a detected marker (upper left). Main idea of precise corner detection is intersecting segment of contour and segment parallel with instrument as a new precise corner point (upper middle). Contour image of the detected marker, and red points are rough corner points (upper right). Green point is an inner corner point (lower left). Blue point is a precise corner point (lower middle). Four precise corner points are derived (lower right).

4.5 Multi-layer Marker Set

From discussions above, markers in a marker set can be detected and be used to calculate transformation matrix. A transformation matrix can be derived using only a detected marker. The purpose of using multi-layer marker set has two: view-invariant and

enhancing precision.

4.5.1 Achieving View-invariant

Ideally, when an image capture device observes a cylinder, there is 180 degrees of cylinder visible. However, parts far form middle region of cylinder cannot be observed completely, may losing some information or compressed. The angle of cylinder in which pattern is located can be observed without losing information is defined as visible angle (θ_v), shown in Fig. 4-17. It's necessary that at least a marker is located in visible angle, so the tracking can work. Nevertheless, a marker located in visible angle originally may locate out of visible angle after the instrument is moved or rotated, which makes tracking can't work normally. That is view-invariant problem.

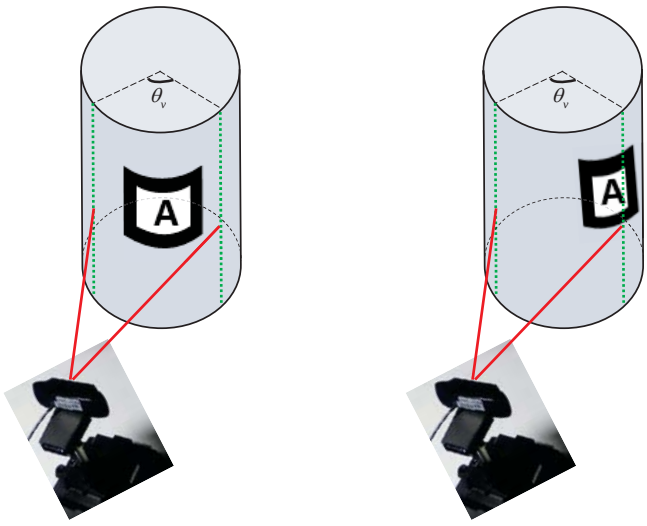

Fig. 4-17 Marker located in visible angle (θ_v) can be observed with complete information (left). Marker located out of visible angle is observed missing some information (right).

To ensure that at least one marker can be observed from any view angle, a multi-layer marker set is adopted. There are two solutions for view-invariant problem. The first is shrinking marker size of each marker so that number of markers on each layer can increase, shown in Fig. 4-18. Hence the possibility that at least one marker can be observed increases. However, the smaller the marker size is, the worse the tracking accuracy is.

Fig. 4-18 Five markers a layer (left). To solve view-invariant problem, one method is adding number of markers on each layer (right).

The second solution is increasing number of marker layers, shown in Fig. 4-19. With increase of marker layers, displacement shift between marker layers is reduced. In one layer case, if a marker is located in visible angle, which means another marker is located in visible angle when the instrument is rotated with angle of a marker on cylinder. In two layer case, displacement shift between two layers is half length of marker side. That means if a marker is located in visible angle, marker on another layer is located in visible

angle when the instrument is rotated with angle of half marker on instrument. And, in third layer case, displacement shift between two layers is 1/3 length of marker side. That means if a marker is located in visible angle, marker on another layer is located in visible angle when the instrument is rotated with angle of 1/3 marker on instrument. In summary, with increase of marker layers, the possibility that at least one marker is located in visible angle increase. However, large number of marker layers may lead to difficulty of marker identification.

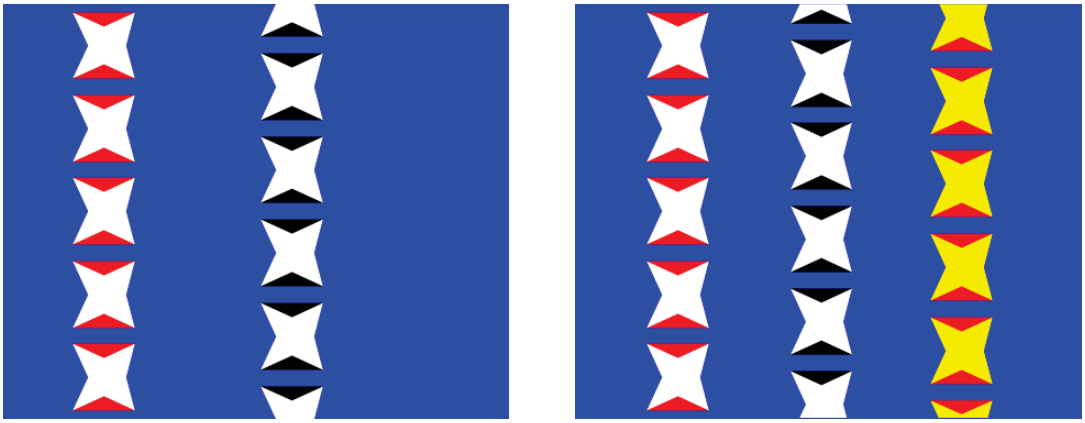

Fig. 4-19 Original marker set design (left). Another method to solve view-invariant problem is adding number of marker layers (right).

Both methods introduced above has problems respectively. Consequently, when designing a marker set, the two method should be traded off. In our design, a practicable version is shown in Fig. 4-20. Markers on layer 1 and markers on layer 2 has a displacement shift of half-length of marker side. Once markers on layer 1 can’t be observed, not located in visible angle, markers on layer 2 can be observed. Thus the

tracking work can achieve normally. The same reason is used for displacement shift between layer 3 and layer 4.

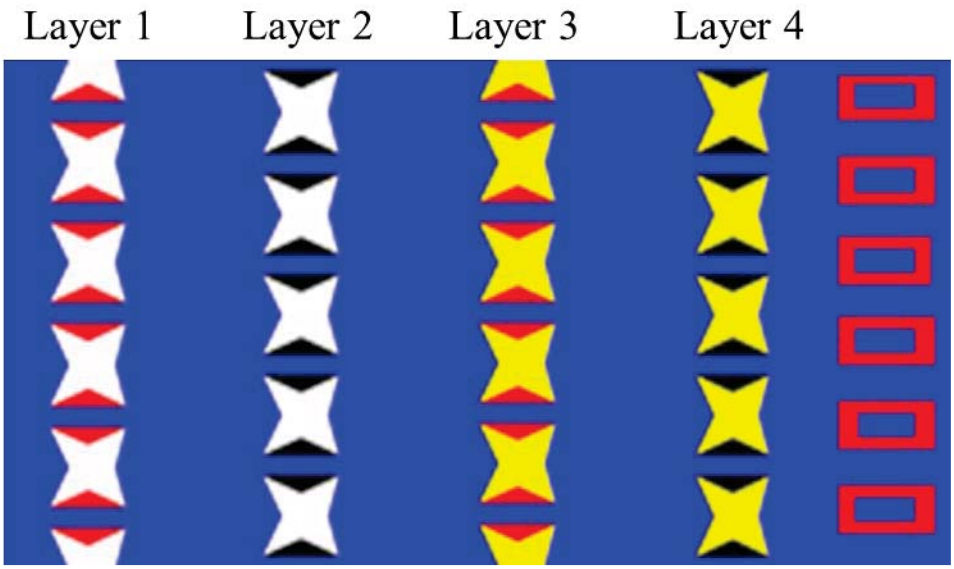

Fig. 4-20 A marker set consists of background region, multi-layer markers and direction rectangles.

4.5.2 Enhancing Tracking Precision

The ARToolkit library has an algorithm to calculate transformation matrix using multiple markers whose relative relations in marker coordinate are known [1, 27]. The main idea is to minimize amount of errors between the actual feature positions in the camera screen coordinate system and the estimated positions which transformed by positions in marker coordinate system.

When multiple markers are used to calculate transformation matrix, the initial transformation matrix is calculated by the marker within maximum area using the method

discussed in section 3.3. And, the optimization is performed. Positions in marker coordinate system can be transformed to positions in camera coordinate system using the transformation matrix obtained. The quality of transformation matrix is evaluated by the sum of difference between the actual feature positions of visible markers in the image (detected) and the estimated positions of visible markers (transformed), shown in (4.1).

$$e = \sum_{i=0}^{n} \left(x_i^{screen,act} - x_i^{screen,est} \right)^2 + \left(y_i^{screen,act} - y_i^{screen,est} \right)^2, \ i \text{ is vertex number} \qquad (4.1)$$

The transformation from marker coordinates to camera coordinates is shown in (4.2) [1], where $C(\cdot)$ means cosine function and $S(\cdot)$ means sine function. The transformation matrix has six independent variables containing rotation component α β γ and translation component $W_x W_y W_z$. In optimization procedure, the variables of rotation component are adjusted with small variances. The variables of translation component can be calculated using the adjusted rotation variables and several coordinates of detected markers by the transformation function in (4.2). And then the error of distance difference in (4.1) is calculated.

$$\begin{bmatrix} X_c \\ Y_c \\ Z_c \\ 1 \end{bmatrix} = \begin{bmatrix} V_{11} & V_{12} & V_{13} & W_x \\ V_{21} & V_{22} & V_{23} & W_y \\ V_{31} & V_{33} & V_{33} & W_z \\ 0 & 0 & 0 & 1 \end{bmatrix} \begin{bmatrix} X_m \\ Y_m \\ Z_m \\ 1 \end{bmatrix}$$
$$= \begin{bmatrix} C(\alpha)\cdot C(\beta) & C(\alpha)S(\beta)S(\gamma) - S(\alpha)\cdot C(\gamma) & C(\alpha)S(\beta)C(\gamma) + S(\alpha)\cdot S(\gamma) & W_x \\ S(\alpha)\cdot C(\beta) & S(\alpha)S(\beta)S(\gamma) + C(\alpha)\cdot C(\gamma) & S(\alpha)S(\beta)C(\gamma) + C(\alpha)\cdot S(\gamma) & W_y \\ -S(\beta) & C(\beta)\cdot S(\gamma) & C(\beta)\cdot C(\gamma) & W_z \\ 0 & 0 & 0 & 1 \end{bmatrix} \begin{bmatrix} X_m \\ Y_m \\ Z_m \\ 1 \end{bmatrix} \qquad (4.2)$$

After testing all the cases of adjusted transformation matrix, the case with minimum error is preserved as the optimized outcome. This optimization method is also used when only one marker is observed. However, the optimization results are more precise when multiple markers are used because there are more points can be used to minimize the error index.

Even though the transformation matrix can be calculated precisely when multiple markers are used, the used markers should be filtered. This procedure is called confident marker decision. Fig. 4-21 shows the procedure after marker detection. In our case, markers in the same layer have no different marker id. Hence, only one marker of them can be used in a frame. Markers in nearby layers, like markers in layer 1 and markers in layer 2, can't be also used in a frame because there are not only one possible relations between them, which would give rise to mistakes of transformation matrix calculation. Markers in different layers can be used only when they are in correspondent layers like layer 1 and layer 3 or layer 2 and layer 4 because they can meet one relation in marker coordinate system.

If there are multiple markers observed, the criterions to filter confident markers has two. First, markers in correspondent layers has high priority because they can be used to calculate transformation matrix more precisely. When multiple combinations, whose markers are all in respondent layers, are visible, the second criterion is to select markers

which the distances between markers and the major axis of background region are smaller. The reason is that markers closer to major axis of major axis contain more pixels, which can enhance the detection precision.

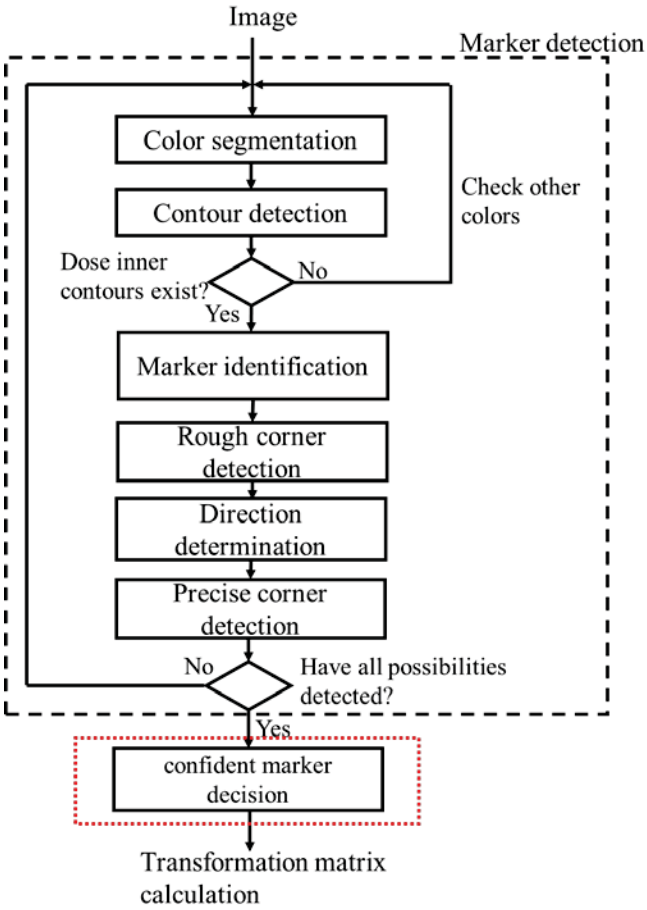

Fig. 4-21 The procedure after marker detection is to decided confident markers for transformation matrix calculation.

In left of Fig. 4-22, multiple markers are visible in the meanwhile. Based on the two criterions discussed above, markers in correspondent layers have high priority. And then distances between markers and major axis of background region, green line in the right

of figure, are calculated. Markers with minimum distances are chosen as the confident markers. The markers whose corner points are marked green in left of the figure are the confident markers of this case.

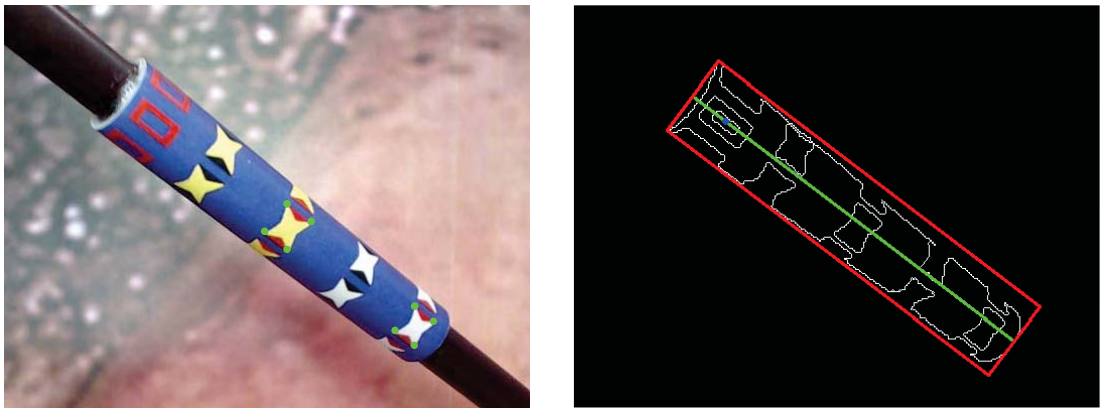

Fig. 4-22 The markers whose corner points are marked green are filtered as the confident markers used to calculate transformation matrix. The criterions to filter confident markers are distances between markers and major axis of background region.

Chapter 5 Experimental Results

The experimental results of the proposed system is presented in this chapter. Because the system is a tracking system with localization function, an experiment to verify the absolute accuracy is needed. A world coordinate is used as reference coordinate. All the estimated positions in camera coordinate system are transformed to world coordinate system. The errors are defined as distances between transformed estimated positions and the correspondent reference positions in world coordinate system. Hence, a calibration between camera coordinate system and world coordinate system is necessary, which is presented in section 5.1. And the absolute accuracy experiment is presented in section 5.2. The specification of software and hardware used in the experiment is shown in Table 5-1.

Table 5-1 Hardware and software specification

Item	Specification
Personal Computer	CPU: Inter® Xeon® CPUE3-1230 V2 @ 3.30GHz
	RAM: 8.00GB
	OS: Window 7 Enterprise 32-bit SP1
Camera	Logitech C920
	Frame Rate: 30 fps
	Image Resolution: 1280*720
Development Environment	Microsoft Visual Studio 2010

5.1 Coordinate System Calibration

The coordinate systems used in the experiment has three: marker coordinate system, camera coordinate system and world coordinate system. A position in marker coordinate system can be transformed into position in camera coordinate system using the transformation matrix from marker coordinate system to camera coordinate system T_m^c calculated by tracking system. To compared with which in world coordinate system, a transformation matrix from camera coordinate system to world coordinate system is needed, so that every estimated point in camera coordinate system can be transformed into position in world coordinate system. To calculate transformation matrix from camera coordinate system to world coordinate system is the main purpose of coordinate system calibration.

5.1.1 Experiment Setup of Coordinate System Calibration

A manufactured panel is used as the world coordinate system, shown in Fig. 5-1. There are many holes with 2 mm diameter on the module. The distances between centers of each two nearby holes is 10 mm. Since the panel is manufactured by mechanical factory, the accuracy of the module is promised less than 0.1 mm, which is accurate enough for being a reference. A fixed point on the lower left of the panel is chose as the origin of world coordinate system. The x-axis is chose parallel with ground. The y-axis is chose vertical to ground. The z-axis is vertical to the panel. Hence, position of each hole in

world coordinate system can be estimated by the relation between each hole and the hole regarded as origin of world coordinate system.

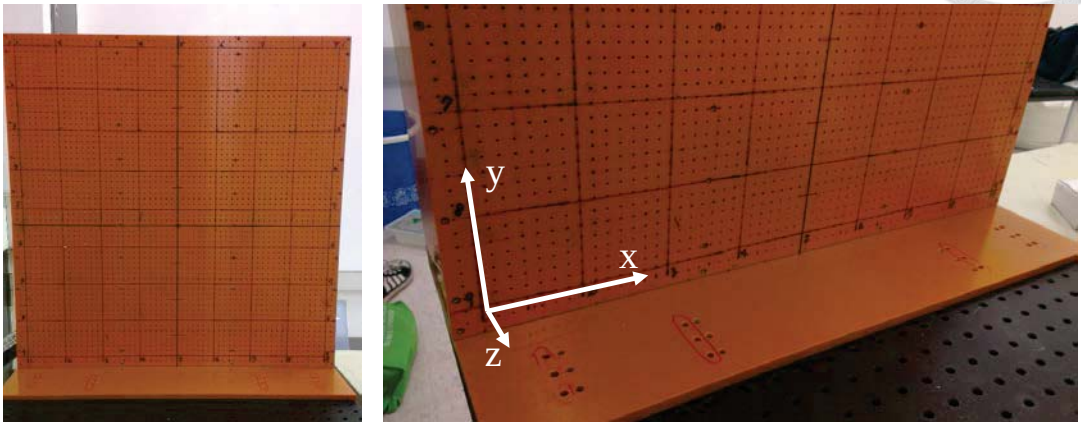

Fig. 5-1 A manufactured module is used as the world coordinate system.

Fig. 5-2 A square marker is attached on a specific position of the panel. When camera catches image with the marker, the position of the marker in camera coordinate can be estimated.

The calibration setup is shown in Fig. 5-2. A square marker is attached on a specific

position of the panel. Center of the marker is aligned with a specific hole on the panel. Hence, position of center of the marker in world coordinate is known, defined as q^w. When the square marker occurs on the image captured by the camera, the position of center of the marker in camera coordinate system, defined as q^c, can be estimated using tracking system of ARToolkit. The transformation between camera coordinates and world coordinates is shown in (5.1), where T_c^w represents the transformation matrix.

$$q^w = T_c^w q^c \tag{5.1}$$

$$\begin{bmatrix} x_w \\ y_w \\ z_w \\ 1 \end{bmatrix} = \begin{bmatrix} r_{11} & r_{12} & r_{13} & t_1 \\ r_{21} & r_{22} & r_{23} & t_2 \\ r_{31} & r_{32} & r_{33} & t_3 \\ 0 & 0 & 0 & 1 \end{bmatrix} \begin{bmatrix} x_c \\ y_c \\ z_c \\ 1 \end{bmatrix} \tag{5.2}$$

Because the transformation from camera coordinates to world coordinates contains rotation component and translation component, (5.1) is equal to (5.2), where each r_{ij} represents parameter of rotation component, and each t_i represents parameter of translation component. Since there are 12 parameters in the transformation matrix, the transformation matrix can be calculated by at least 4 sets of known points in the two coordinate systems respectively using (5.3) and (5.4), where superscript T means transpose.

$$T_c^w = q^w inv\left(q^c\right), \text{ if } inv\left(q^c\right) \text{ exists.} \tag{5.3}$$

$$inv\left(q^c\right) = \left(q^c\right)^T inv\left(q^c \left(q^c\right)^T\right), \text{ if } q^c \left(q^c\right)^T \text{ is nonsingular.} \tag{5.4}$$

After the transformation matrix is calculated, the quality of the transformation matrix

is verified by the error index shown in (5.5), which is distance between each reference position in world coordinate system and the transformed position in world coordinate system from estimated position in camera coordinate system.

$$error = \left\| q_{w,\text{est}} - q_{w,trans} \right\| \tag{5.5}$$

5.1.2 Experimental Results of Coordinate System Calibration

To enhance the calibration precision, in this calibration procedure, 26 set of points was used to calculate the transformation matrix from camera coordinates to world coordinates. Table 5-2 shows the experiment results, where xw_ref, yw_ref, zw_ref mean the position of marker center in world coordinate system derived by the holes on the panel directly, and xw_est, yw_est, zw_est mean the position in world coordinate system transformed from estimated position of marker center in camera coordinate system. The mean error of coordinate calibration is 0.6 mm, and the standard deviation is 0.1 mm. The calculated transformation matrix was used for the accuracy experiment presented in section 5.2.

Table 5-2 Error of coordinate calibration

Coordinate calibration (unit: mm)						
xw_ref	yw_ref	zw_ref	xw_est	yw_est	zw_est	error
180.0	110.0	0.0	179.9	109.5	-0.1	0.5
120.0	80.0	0.0	120.2	79.8	-0.6	0.7
150.0	80.0	0.0	150.1	80.0	-0.5	0.5
180.0	110.0	10.0	180.1	109.9	10.4	0.5
120.0	80.0	10.0	120.2	80.3	9.6	0.6
150.0	80.0	10.0	150.2	80.4	9.8	0.5
90.0	80.0	10.0	89.8	79.6	10.2	0.5
130.0	110.0	10.0	129.9	110.1	9.6	0.4
170.0	80.0	10.0	169.7	79.7	10.2	0.5
90.0	80.0	0.0	89.8	79.8	0.9	0.9
130.0	110.0	0.0	130.0	110.5	0.1	0.5
170.0	80.0	0.0	169.8	80.3	0.4	0.6
					avg error	0.6
					std	0.1

5.2 Accuracy Experiment

Because the transformation matrix from camera coordinates to world coordinates is calculated in the calibration procedure, every estimated position in camera coordinate system can be transformed into estimated position in world coordinate system.

5.2.1 Experiment Setup of Accuracy Experiment

The experiment setup is shown in Fig. 5-3. In the experiment setup, the instrument tip should be fixed to the hole on the panel, so that the reference position of instrument tip in world coordinate system can be derived by relationship between the hole and the panel. The camera is settled on a specific position and adjusted an appropriate pose. In

the experiment procedure, the camera remains fixed position to ensure the transformation matrix from camera coordinates to world coordinate doesn't change.

Fig. 5-3 The experiment setup of accuracy experiment.

The manufactured panel and the camera used in this experiment are the same with which introduced in section 5.1. A manufactured acrylic block is used to fix the instrument with marker module rigidly to the panel, shown in Fig. 5-4. One end of a bolt is penetrated into the center of instrument, and the other end of the bolt is penetrated into a hole of the panel, which can assure that the position of instrument tip is regarded as the position of the penetrated hole. Another two bolts are used to fix the acrylic block to the panel by penetrating another two holes. The main use the acrylic block is to reduce the deformation of instrument due to the torque applied to the instrument tip.

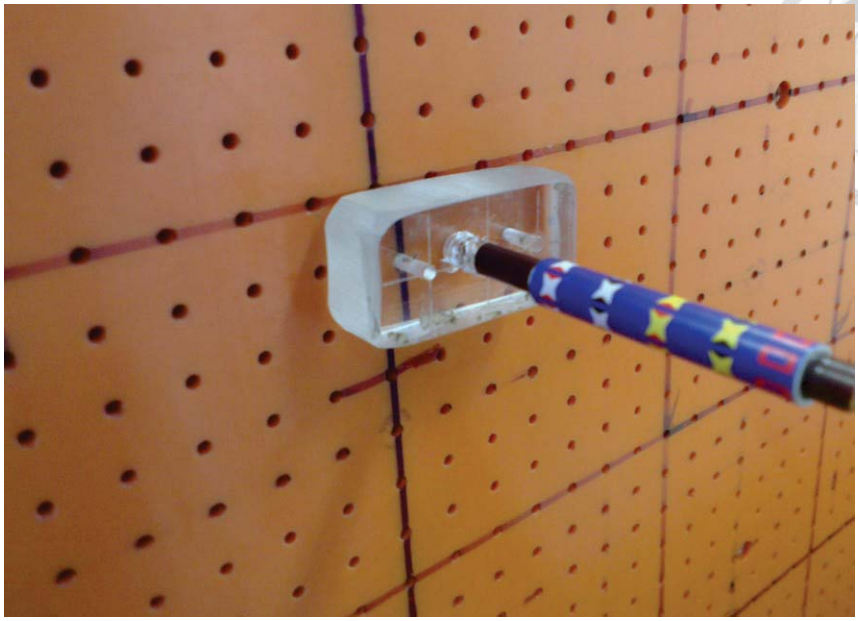

Fig. 5-4 A manufactured acrylic block with bolts is used to fixed the instrument with marker module rigidly to the panel.

The cylindrical marker set on the marker module can be detected by the tracking system, and the position of marker set in camera coordinate system can be estimated, shown in Fig. 5-5. Because the relative positions between marker set and instrument tip is known, the position of instrument tip q_{ref}^{w} can be estimated using transformation matrix calculated using the marker set. And then the estimated position of instrument tip in world coordinate system q_{est}^{w} can be derived using the transformation matrix from camera coordinates to world coordinates, shown in (5.6).

$$q_{est}^{w} = T_{c}^{w} q_{est}^{c} \tag{5.6}$$

The accuracy error is defined as distance between the reference position of instrument tip q_{ref}^{w} in world coordinate system and the estimated position of instrument

tip q_{est}^{w} in world coordinate system, shown in (5.7).

$$error = \left\| {q_{ref}}^{w} - {q_{est}}^{w} \right\| \tag{5.7}$$

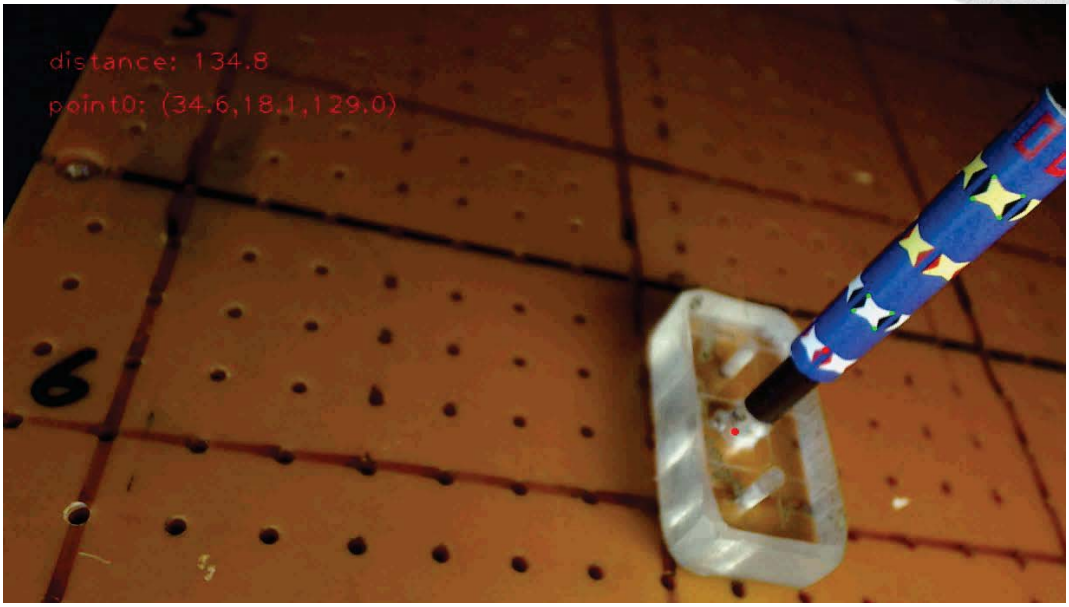

Fig. 5-5 When marker set is detected, the position of instrument tip in camera coordinate system can be estimated.

5.2.2 Experimental Results of Accuracy Experiment

The accuracy of tracking system using cylindrical marker is verified in observation distance from 75 to 150 mm, which is similar with observation distance in minimally invasive surgery. The experiment results is shown in Table 5-3. The mean error of this experiment is 2.7 mm. The standard deviation is 1.0 mm.

Table 5-3 Mean error of accuracy experiment in different observation distance

Distance(mm)	75-80	80-85	85-90	90-95	95-100	100-105	105-110	110-115
Error(mm)	2.0	1.8	2.3	2.2	2.2	2.2	2.1	1.8
Distance(mm)	115-120	120-125	125-130	130-135	135-140	140-145	145-150	
Error(mm)	2.6	1.9	2.7	3.1	3.2	3.6	6.0	

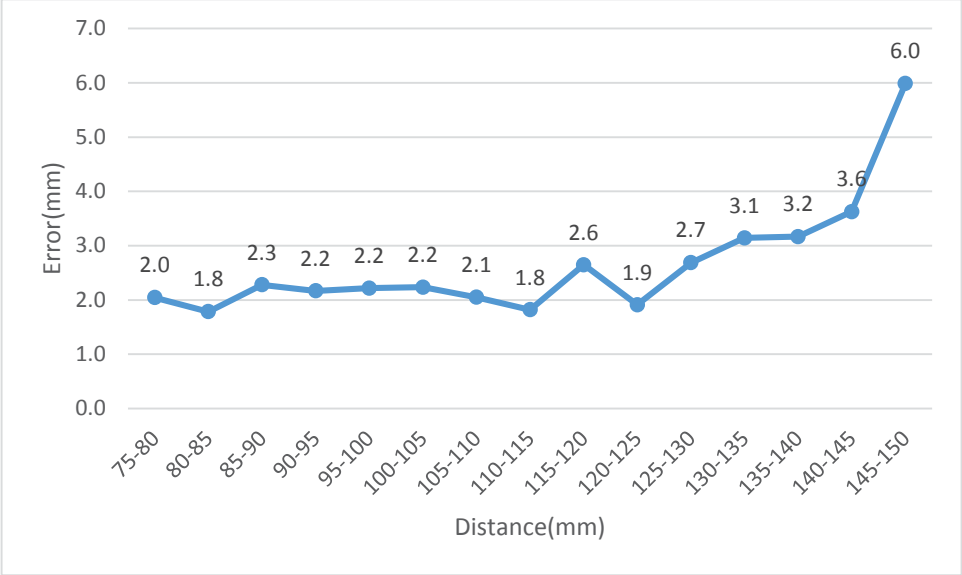

Fig. 5-6 Error of accuracy experiment in different observation distance.

5.3 Discussions

The experiment data shows that the mean errors raise increasingly with the increase of observation distance. The reason is that with the increase of observation distance, the area which each pixel represents reduced progressively. In observation distance of 75 mm, side length of a pixel represents 0.08 mm. In observation distance of 140 mm, side length of a pixel represents 0.14 mm. In other words, the marker can be observed more clearly

in shorter observation distance. The data shows that the accuracy of tracking system can tracks targets in observation distance from 7.5 mm to 140 mm is enough for use in minimally invasive surgery, which is less than the maximal safe distance: 20 mm in minimally invasive surgery.

5.4 Comparison

There is the comparison of tracking technologies. Four benchmarks are chose for comparison [3, 7, 12, 25]. Extracorporeal tracking contains robot kinematics and optical tracking. Intracorporeal tracking contains electromagnetic tracking and optical tracking. The comparison is shown in Table 5-4.

Compared with other tracking technologies, the tracking accuracy of the proposed approach is similar to which of other tracking technologies. The proposed approach preserves advantages of intracorporeal optical tracking, including no ferromagnetic interference, shorter observation distance and simpler coordinate system for coordinate transformation. Moreover, intracorporeal optical tracking using square marker may lead to damages to tissues in surgery, but our proposed approach do not.

Table 5-4 Comparison of tracking technologies

Sensor placement	Extracorporeal tracking		Intracorporeal tracking		
Approach	Robot kinematics 2005 J. Leven [12]	Optical tracking 2008 M. Feuerstein [3]	Electromagnetic tracking 2011 C. T. Yeo [25]	Optical tracking (square marker) 2013 M. C. Ke [7]	Proposed approach
Mean error	2.2 mm	2.6 mm	2.3 mm	1.1 mm	2.7 mm
Ferromagnetic interference	No	No	Yes	No	No
Visibility problem	No	Yes	No	Yes	Yes
Operation interference	Yes	Yes	No	No	No
Damages to tissues	No	No	No	Yes	No
Cost (USD)	Millions	Tens of thousands	Tens of thousands	Hundreds	Hundreds

Chapter 6 Conclusions and Future Work

An intracorporeal optical tracking system using cylindrical marker for minimally invasive surgery is proposed in this thesis. It can be used to track instruments to which cylindrical markers are affixed. Based on original intracorporeal optical tracking system, the shape of marker is improved from square to cylinder. Moreover, a specific marker detection algorithm used to detect cylindrical marker and extract features from cylindrical marker is proposed. In the accuracy experiment, the absolute mean error compared with world coordinate system is 2.7 mm in observation distance from 75 mm to 150 mm.

In this thesis, the coordinate system used in tracking system is camera coordinate system, which is endoscope in minimally invasive surgery. In the future work, a mechanism to understand the motion of endoscope is needed. Because the endoscope moves frequently in surgery, the transformation between endoscope coordinate and world coordinate changes with the motion of endoscope. With the mechanism, the endoscope coordinate system can be calibrated with other coordinate system so as to achieve other applications which need coordinate transformation with endoscope system.

REFERENCES

[1] H. Kato and M. Billinghurst, "Marker tracking and HMD calibration for a video-based augmented reality conferencing system," in *Augmented Reality, 1999. (IWAR '99) Proceedings. 2nd IEEE and ACM International Workshop on*, 1999, pp. 85-94.

[2] C. Bichlmeier, S. M. Heining, M. Feuerstein, and N. Navab, "The Virtual Mirror: A New Interaction Paradigm for Augmented Reality Environments," *Medical Imaging, IEEE Transactions on,* vol. 28, pp. 1498-1510, 2009.

[3] M. Feuerstein, T. Mussack, S. M. Heining, and N. Navab, "Intraoperative Laparoscope Augmentation for Port Placement and Resection Planning in Minimally Invasive Liver Resection," *Medical Imaging, IEEE Transactions on,* vol. 27, pp. 355-369, 2008.

[4] D. Burschka, J. Corso, M. Dewan, W. Lau, M. Li, H. Lin, *et al.*, "Navigating inner space: 3-D assistance for minimally invasive surgery," *Robotics and Autonomous Systems,* vol. 70, 2005.

[5] G. Lacey, D. Ryan, D. Cassidy, and D. Young, "Mixed-Reality Simulation of Minimally Invasive Surgeries," *IEEE MultiMedia,* vol. 14, pp. 76-87, 2007.

[6] D. Sindram, I. H. McKillop, J. B. Martinie, and D. A. Iannitti, "Novel 3-D laparoscopic magnetic ultrasound image guidance for lesion targeting," *HPB,* vol. 12, pp. 709-716, 2010.

[7] K. Ming-Chun, T. Yen-Hsiang, C. Cheng-Wei, H. Ming-Chih, L. Feng-Li, Y. Jia-Yush, *et al.*, "Preliminary study of intracorporeal localization for endoscopy tracking," in *Automatic Control Conference (CACS), 2013 CACS International*, 2013, pp. 130-134.

[8] T. Langø, S. Vijayan, A. Rethy, C. Våpenstad, O. Solberg, R. Mårvik, *et al.*, "Navigated laparoscopic ultrasound in abdominal soft tissue surgery: technological overview and perspectives," *International Journal of Computer Assisted Radiology and Surgery,* vol. 7, pp. 585-599, 2012/07/01 2012.

[9] H. Azimian, J. Breetzke, A. L. Trejos, R. V. Patel, M. D. Naish, T. Peters, *et al.*, "Preoperative planning of robotics-assisted minimally invasive coronary artery bypass grafting," in *Robotics and Automation (ICRA), 2010 IEEE International Conference on,* 2010, pp. 1548-1553.

[10] L. Jianmin, W. Shuxin, W. Xiaofei, H. Chao, and Z. Lin'an, "Development of a novel mechanism for minimally invasive surgery," in *Robotics and Biomimetics (ROBIO), 2010 IEEE International Conference on*, 2010, pp. 1370-1375.

[11] J. Li, S. Wang, X. Wang, and C. He, "Optimization of a novel mechanism for a minimally invasive surgery robot," *The International Journal of Medical Robotics and Computer Assisted Surgery*, vol. 6, pp. 83-90, 2010.

[12] J. Leven, D. Burschka, R. Kumar, G. Zhang, S. Blumenkranz, X. Dai, *et al.*, "DaVinci Canvas: A Telerobotic Surgical System with Integrated, Robot-Assisted, Laparoscopic Ultrasound Capability," in *Medical Image Computing and Computer-Assisted Intervention – MICCAI 2005*. vol. 3749, J. Duncan and G. Gerig, Eds., ed: Springer Berlin Heidelberg, 2005, pp. 811-818.

[13] J. de Siebenthal and F. Langlotz, "Use of a new tracking system based on ArToolkit for a surgical simulator: accuracy test and overall evaluation," in *Augmented Reality Toolkit, The First IEEE International Workshop*, 2002, p. 6 pp.

[14] R. Shahidi, M. R. Bax, C. R. Maurer, Jr., J. A. Johnson, E. P. Wilkinson, W. Bai, *et al.*, "Implementation, calibration and accuracy testing of an image-enhanced endoscopy system," *Medical Imaging, IEEE Transactions on*, vol. 21, pp. 1524-1535, 2002.

[15] J. Chen, Y. Wang, Y. Liu, and D. Weng, "Navigating System for Endoscopic Sinus Surgery Based on Augmented Reality," in *Complex Medical Engineering, 2007. CME 2007. IEEE/ICME International Conference on*, 2007, pp. 185-188.

[16] L. Hongen, T. Inomata, I. Sakuma, and T. Dohi, "3-D Augmented Reality for MRI-Guided Surgery Using Integral Videography Autostereoscopic Image Overlay," *Biomedical Engineering, IEEE Transactions on*, vol. 57, pp. 1476-1486, 2010.

[17] K. A. Gavaghan, M. Peterhans, T. Oliveira-Santos, and S. Weber, "A Portable Image Overlay Projection Device for Computer-Aided Open Liver Surgery," *Biomedical Engineering, IEEE Transactions on*, vol. 58, pp. 1855-1864, 2011.

[18] V. Lahanas, C. Loukas, N. Nikiteas, D. Dimitroulis, and E. Georgiou, "Psychomotor skills assessment in laparoscopic surgery using augmented reality scenarios," in *Digital Signal Processing (DSP), 2011 17th International Conference on*, 2011, pp. 1-6.

[19] Q. He, N. Wei, B. Li, C. Hu, and M. Q. H. Meng, "Marker-based quadri-ocular tracking system for surgery," *Computer Vision, IET*, vol. 6, pp. 435-441, 2012.

[20] H. Delingette, X. Pennec, L. Soler, J. Marescaux, and N. Ayache, "Computational Models for Image-Guided Robot-Assisted and Simulated Medical Interventions," *Proceedings of the IEEE*, vol. 94, pp. 1678-1688, 2006.

[21] J. Harms, H. Feussner, M. Baumgartner, A. Schneider, M. Donhauser, and G. Wessels, "Three-dimensional navigated laparoscopic ultrasonography: first experiences with a new minimally invasive diagnostic device," *Surg Endosc*, vol. 15, pp. 1459-62, Dec 2001.

[22] V. Martens, S. Schlichting, A. Besirevic, and M. Kleemann, "LapAssistent — a laparoscopic liver surgery assistance system," in *4th European Conference of the International Federation for Medical and Biological Engineering*. vol. 22, J. Vander Sloten, P. Verdonck, M. Nyssen, and J. Haueisen, Eds., ed: Springer Berlin Heidelberg, 2009, pp. 121-125.

[23] O. V. Solberg, T. Langø, G. A. Tangen, R. Mårvik, B. Ystgaard, A. Rethy, *et al.*, "Navigated ultrasound in laparoscopic surgery," *Minimally Invasive Therapy & Allied Technologies*, vol. 18, pp. 36-53, 2009.

[24] M. Feuerstein, T. Reichl, J. Vogel, J. Traub, and N. Navab, "Magneto-Optical Tracking of Flexible Laparoscopic Ultrasound: Model-Based Online Detection and Correction of Magnetic Tracking Errors," *Medical Imaging, IEEE Transactions on*, vol. 28, pp. 951-967, 2009.

[25] C. T. Yeo, T. Ungi, P. U-Thainual, A. Lasso, R. C. McGraw, and G. Fichtinger, "The Effect of Augmented Reality Training on Percutaneous Needle Placement in Spinal Facet Joint Injections," *Biomedical Engineering, IEEE Transactions on*, vol. 58, pp. 2031-2037, 2011.

[26] S. Speidel, E. Kuhn, S. Bodenstedt, S. Röhl, H. Kenngott, B. Müller-Stich, *et al.*, "Visual tracking of da Vinci instruments for laparoscopic surgery," 2014, pp. 903608-903608-6.

[27] H. Kato, M. Billinghurst, I. Poupyrev, K. Imamoto, and K. Tachibana, "Virtual object manipulation on a table-top AR environment," in *Augmented Reality, 2000. (ISAR 2000). Proceedings. IEEE and ACM International Symposium on*, 2000, pp. 111-119.